UNIVERSITÀ DEGLI STUDI DI BOLOGNA

ALMA MATER STUDIORUM

ANNO ACCADEMICO 2007/2008

TESI DI DOTTORATO IN GEOFISICA

XX CICLO

Shallow and deep deformation in northern Apennines region using seismological data

Candidato:

Simone Salimbeni

Tutore:

Dr.ssa Silvia Pondrelli

Contents

INTRODUCTION **5**

1 THE NORTHERN APENNINES AND ITS MAIN FEATURES **7**

1.1 WHY THE APENNINES? 7

1.2 GEOLOGICAL FRAMEWORK 8

1.3 SEISMICITY, STRESS AND DEFORMATION IN THE NORTHERN APENNINES 9

1.4 DEEP STRUCTURE BENEATH THE NORTHERN APENNINES 13

2 SHALLOW DEFORMATION **15**

2.1 DATA DETERMINATION: SEISMIC MOMENT TENSOR, CMT AND RCMT 16

2.1.1 THE UPDATE OF THE EUROPEAN-MEDITERRANEAN RCMT CATALOG IN THE ITALIAN REGION: THE ITALIAN CMT DATASET 18

2.2 SEISMIC DEFORMATION THROUGH MOMENT TENSOR SUMMATION 24

2.3 DISCUSSION ON SHALLOW DEFORMATION RESULTS 24

3 DEFORMATION AT DEPTH - MANTLE DEFORMATION **31**

3.1 SEISMIC ANISOTROPY 31

3.2 SHEAR WAVE SPLITTING 33

3.3 METHOD AND DATA 35

3.4 MEASUREMENTS AND ANISOTROPIC DOMAINS 36

3.5 ANISOTROPY VARIATION AT DEPTH 45

4 MODELING COMPLEX ANISOTROPIC STRUCTURES **49**

4.1 CROSS-CONVOLUTION METHOD: A TWO LAYERS STRUCTURE 50

4.1.1 DATASET USED 51

4.1.2 RESULTS FOR A TWO ANISOTROPIC LAYERS MODEL 54

5 DISCUSSION AND CONCLUSIONS: A CASE OF OBLIQUE TRENCH RETREAT 57

BIBLIOGRAPHY 63

ACKNOWLEDGMENTS 75

INTRODUCTION

For its particular position and the complex geological history, the Northern Apennines has been considered as a natural laboratory to apply several kinds of investigations. By the way, it is complicated to joint all the knowledge about the Northern Apennines in a unique picture that explains the structural and geological emplacement that produced it. The main goal of this thesis is to put together all information on the deformation - in the crust and at depth - of this region and to describe a geodynamical model that takes account of it.

To do so, we have analyzed the pattern of deformation in the crust and in the mantle. In both cases the deformation has been studied using always information recovered from earthquakes, although using different techniques. Our results are compared and added to those of other geophysical studies.

This thesis is therefore composed by two main parts. First, we studied the pattern of seismic deformation. We started looking for the information recovered by seismic moment tensors. One of the most famous technique to calculate a seismic moment tensor is that named Centroid Moment Tensor (CMT) (DZIEWONSKI ET AL., 1981). It has been developed in a time span of about 20 years and it is commonly used to compute CMTs for worldwide earthquakes with M greater than 5.5 that are included in the Global CMT Catalog. Recently, ARVIDSSON AND EKSTRÖM (1998) have modified this procedure allowing the use in the inversion not only of body waves but also of surface waves to be able to determine seismic source parameters for earthquakes with smaller magnitude (down to $Mw > 4.0$). We applied this important seismological tool in areas characterized by moderate seismicity as the Northern Apennines. Through this activity we have built up the Italian CMT dataset (PONDRELLI ET AL., 2006) from which we have selected all the available moment tensors for our study region. On this dataset we computed the pattern of seismic deformation using the KOSTROV (1974) method on a regular grid of 0.25 degree cells. We obtained a map of lateral variations of the pattern of seismic deformation on different layers of depth, taking into account the fact that shallow earthquakes (within 15 km of depth) in the region occur everywhere while most of events with a deeper hypocenter (15-40 km) occur only in the outer part of the belt, on the Adriatic side.

The second part of this thesis consisted in the analysis of the deep deformation, i.e. that occurred in the mantle. To do this we studied the seismic anisotropy characterizing the structure below the Northern Apennines. In the crust the anisotropy is due to the presence of aligned fluid filled cracks or alternating isotropic layers with different elastic properties; in the mantle the most important cause of seismic anisotropy is the lattice preferred orientation (LPO) of the mantle minerals as the olivine. This last is a highly anisotropic mineral and tends to align its fast crystallographic axes (a-axis) parallel to the astenospheric flow as a response to finite strain induced by geodynamic processes. The seismic anisotropy pattern of a region is measured utilizing the shear wave splitting phenomenon (that is the seismological analogue to optical birefringence). Here, to do so, we apply on teleseismic earthquakes recorded on stations located in the study region, the ŠILENÝ AND PLOMEROVÁ (1996) approach. The results are analyzed on the basis of their lateral and vertical variations to better define the earth structure beneath Northern Apennines. We find different anisotropic domains, a Tuscany and an Adria one, with a pattern of seismic anisotropy which laterally varies in a similar way respect to the seismic deformation. Moreover, beneath the Adriatic region the distribution of the splitting parameters is so complex to request an appropriate analysis. Therefore we applied on our data the code of MENKE AND LEVIN (2003) which allows to look for different models of structures with multilayer anisotropy. We obtained that the structure beneath the Po Plain is probably even more complicated than expected.

On the basis of the results obtained for this thesis, added with those from previous works, we suggest that slab roll-back, which created the Apennines and opened the Tyrrhenian Sea, evolved in the north boundary of Northern Apennines in a different way from its southern part. In particular, the trench retreat developed primarily south of our study region, with an eastward roll-back. In the northern portion of the orogen, after a first stage during which the retreat was perpendicular to the trench, it became oblique with respect to the structure.

Chapter 1

THE NORTHERN APENNINES AND ITS MAIN FEATURES

1.1 WHY THE APENNINES?

Synorogenic and late orogenic extension has been recognized in many convergent orogens, including Himalayas (MOLNAR ET AL., 1993), the Cyclades of the Aegean (LISTER ET AL., 1984), the Hellenic subduction wedge (JOLIVET ET AL., 1996), the European Alps (REDDY ET AL., 1999) and the Apennines (MALINVERNO AND RYAN, 1986; CARMIGNANI ET AL., 1994; JOLIVET ET AL., 1998). Considering the different tectonic styles of all these areas, it would be simplistic to assume that a single geodynamic model would explain all instances of extension in a convergent environment. For example the extension occurs as orogen-parallel in Tibetan plateau, but in the Apennines it is perpendicular to the chain.

One of the most interesting model, used to explain the extension in the Apennines and in the Hellenic orogenic system, is the roll-back of a subducting slab (DEWEY, 1980; DOGLIONI, 1991; ROYDEN, 1993). In this model, the subducting plate roll-backs away from the overriding plate and induces crustal extension and mantle flow in the upper plate. This mechanism is the continental analogue to back-arc rifting related to Mariana-style subduction system. In oceanic environment the ranges of the extension is greater than in continental one (about 200 Km from the trench in oceanic systems and from 50 to 85 Km in continental one), so in this last, extension and compression lives in a narrow range that provides the results more complex. Given that the Hellenic wedge is completely submerged while the Apenninic wedge, mainly in the Northern part, lives completely above the water, the Apenninic system could be a natural laboratory to study the slab-retreat mechanism in the continental region. For this reasons our study will focus on the northernmost part of the belt.

1.2 GEOLOGICAL FRAMEWORK

The Mediterranean region represents the western termination of the Alpine-Himalayan tectonic system. It has been shaped during the last 100 My by collision of Africa and Arabia with Eurasia, in a process also involving some minor plates, such as Adria, Anatolia and Iberia. In the central part of the Mediterranean region is located the Apennines chain. It developed since the Late Cretaceous via the fast slab roll-back and coeval opening of Tyrrhenian Sea back-arc basin. 35 My ago (Figure 1.1), a continuous trench oriented NE-SW connecting the southern Iberia to the Ligurian region was active (DEWEY ET AL., 1989) and a NW dipping subduction of the Jurassic oceanic basin started (FACCENNA ET AL., 2004). The rifting and spreading of the Liguro-Provencal basin (from 30 My) allowed the migration of the trench in SE to E direction. In the former Italian region from 5 My onward (Figure 1.1) the continuity of the trench was broken and the differential retreating directions induced the separation of the Apenninic front into two main arcs, the Calabrian to the south and the Northern Apennines arc to the north (PATACCA ET AL., 1990). The latter is our area of study.

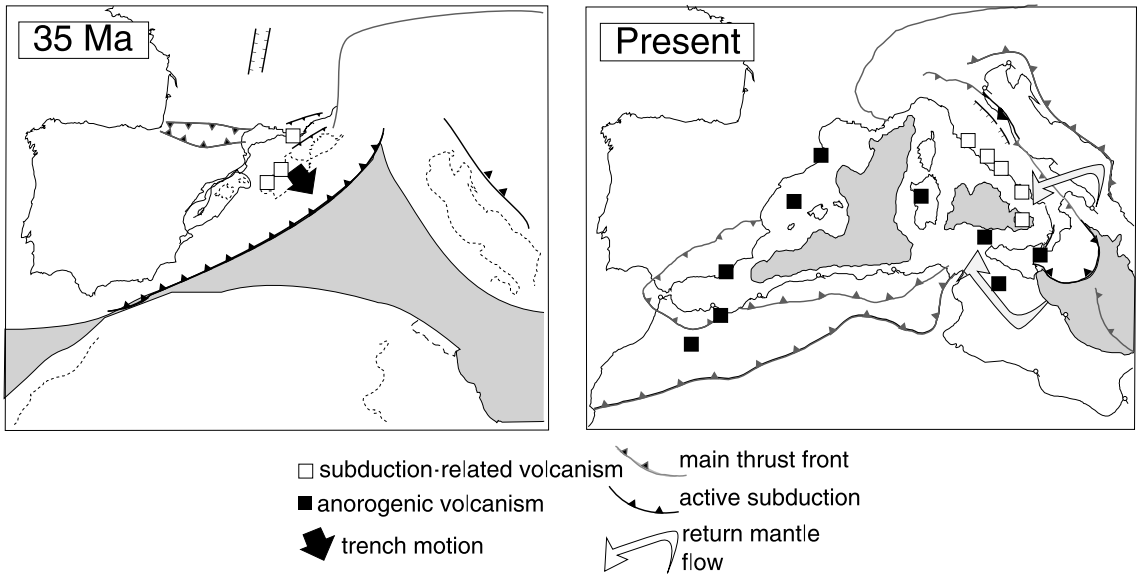

Figure 1.1: Reconstruction of the evolution of the Mediterranean arcs during the last 35 My to present day. The reference frame foresees Eurasia plate as fixed (from FACCENNA ET AL., 2004).

The Northern Apennines wedge formed in the last 30 My. It growth by underplating of deep-water turbidites, olistostromes and crustal rocks. The turbidites were deposited in a series of foredeeps that from late Oligocene to Late Miocene developed in front of the wedge (Macigno, Cervarola, Marnoso-Arenacea basins, RICCI-LUCCHI, 1986; Figure 1.2) and that now outcrop in the eastern side of the belt. In the western part of the area the accretionary wedge is overlapped by Ligurian Lid (green parts in Figure 1.2) and remnants of ophiolite crust and flysh. Locally these are overlained by youngest

Epiligurian marine sediments (Late Eocene to Pliocene, ORI AND FRIEND, 1984; yellow in Figure 1.2) deposited in wedge-top basins as piggyback sequences (ORI AND FRIEND, 1984). The accretionary wedge becomes emergent at about 5 My as it overran the passive margin of Adriatic continental platform. This occurred with a slow convergence rate between the plates (4-5 Km/My) estimated from balanced cross-section (BALLY ET AL., 1986; HILL AND HAYWARD, 1988) and in agreement with the plate tectonics reconstruction of DEWEY ET AL. (1989).

The structural and tectonic setting of the Northern Apennines is strictly related to its complex geological history (Figure 1.2). Southeast of the crest, in the Tyrrhenian flank of the orogen, the geodynamic domain is extensional with the presence of quasi-vertical or medium-high angle normal faults confirming extensional basins (e.g. the Mugello basin). All these faults have Apenninic strike and, given the arcuate form of the chain, the extension area becomes greater moving toward south. Low-angle normal faults seem to be associated with the Cenozoic exhumation of methamorphics rocks (28 Km depth, JOLIVET ET AL., 1998), that generate the Tuscan methamorphics complex and that are represented by the Alpi Apuane (CARMIGNANI AND KLIGFIELD, 1990; CARMIGNANI ET AL., 1994; in blue on Figure 1.2). In the northeastern part of the chain, in the Po-Adriatic side, the structural and tectonic style changes and compressive structures occurs. All the structures are oriented in NW-SE direction coherently with general Apenninic strike. They are related to the shortening of the Po-Adriatic front, composed by 3 main buried arcs that from W to E are named Monferrato, Emilia (AE in Figure 1.2) and Ferrara Romagna arcs (AF-R in Figure 1.2). Beneath the Adriatic Sea the Po-Adriatic front continues and is composed by the Adriatic folds and the Adriatic ridge (AF in Figure 1.2; SCROCCA ET AL., 2007).

1.3 SEISMICITY, STRESS AND DEFORMATION IN THE NORTHERN APENNINES

The structural and tectonics evidences described in the previous section are confirmed by several geophysical data.

The Northern Apennines is affected by a relatively high rate of seismicity. Plotting the hypocenters for earthquakes occurring in the Italian Peninsula, recorded by the Italian Seismic Network of the INGV in 20 years of time, CHIARABBA ET AL. (2005) depicted the characteristics of seismicity distribution (Figure 1.3). Upper crustal seismicity, located in the first 6-8 Km of depth, is located mainly in correspondence of the crest of the chain where NE-trending extension is also detected (WESTAWAY, 1992; MONTONE ET AL., 1999). Subcrustal and deep seismicity in Northern Apennines is instead located mainly in outer part on the chain. In this region the depth is typically between 12 and 25 Km,

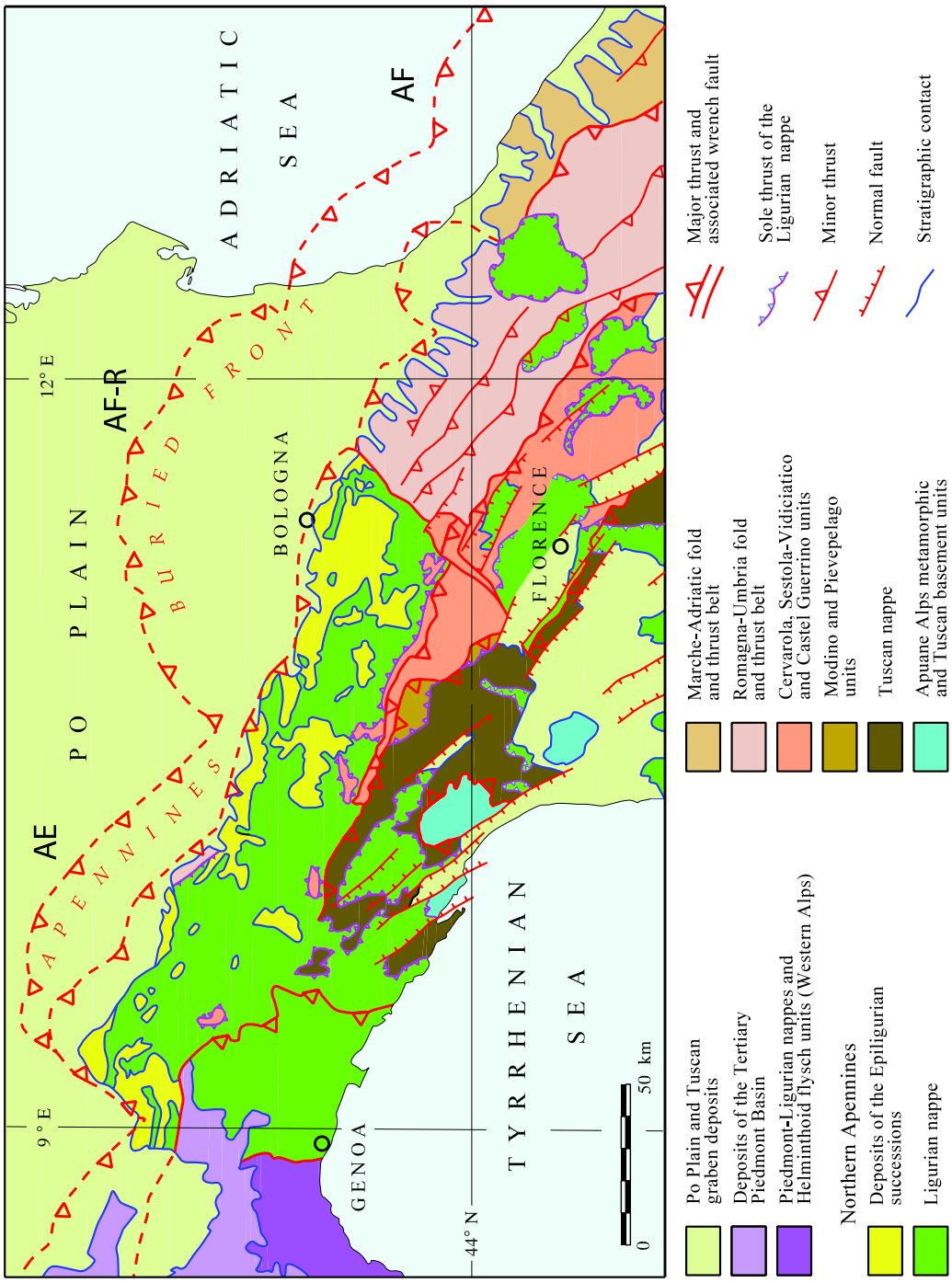

Figure 1.2: Simplified geologic map of the Northern Apennines, from G.A. PINI, (1999) modified. AE=Emilia arc, AF-R=Ferrara-Romagna arc, AF=Adriatic fold.

but also events with greater depth have been found (geq 90 Km; SELVAGGI AND AMATO, 1992). The distribution of the hypocenters allow to draw the flexure of the Adria lithosphere beneath the European one (Figure 1.3; CHIARABBA ET AL., 2005).

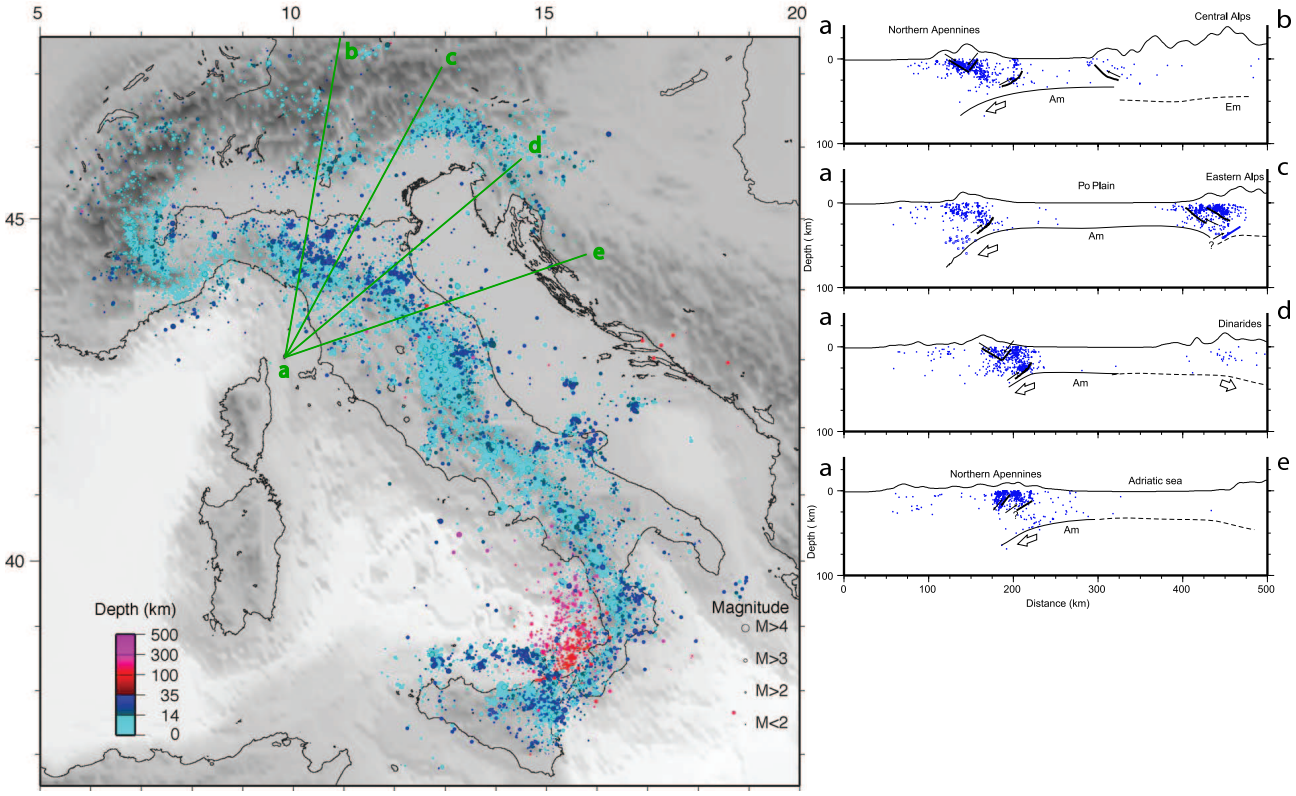

Figure 1.3: Hypocentral distribution of Italian earthquakes (from CHIARABBA ET AL., 2005 modified). Color scale indicates the depth of events (blue colors for the crustal seismicity and red colors for the mantle seismicity). The different size of circles is given by the magnitude scale indicated on the lower right corner. Vertical sections of seismicity across the northern Apenninic arc (in green on the main map) are located on the right. Events falling in 20 km from the section are plotted. The lines indicate the geometry of the Adriatic (Am) and European Moho (Em), also suggested by seismic reflection data and earthquake hypocenters. The bold lines show a simplified sketch of the main faults in the crust.

Other seismological information can be recovered by moment tensor data. The distribution of the seismic moment tensors from the Global CMT Catalog (*www.globalcmt.org*) and from the European-Mediterranean Catalog of the INGV (*http://www.ingv.bo.it/RCMT/*; PONDRELLI ET AL., 2002, 2004A, 2007) evidences how in the inner part of the chain (Tuscany) and along the crest most of the focal mechanisms are extensive, with T-axes oriented perpendicular to the strike of the belt. At the same time, in the eastern side (Po-Plain and Adriatic Sea) moment tensors have a compressional regime with orientations of P-axes in NE-SW directions. Similar results have been obtained by FREPOLI AND AMATO (1997) that calculated focal mechanisms of earthquakes with small-moderate magnitude ($2.6 \leq M_d \leq 4.8$). They

defined two separated deformation zones, very close each other, with a partial overlap in Emilia-Tuscany Apennines. They found that in the external part of the chain the seismicity is characterized by NE-SW compression (σ_1 horizontal and oriented N45°E) while a normal faulting with $\sigma_3 \approx$ E-W is present in the inner part (Tuscany) of it.

Jointing the data recovered by borehole breakout data, centroid moment tensor, fault slip and microearthquakes data, MONTONE ET AL. (1999, 2004) inferred the present-day stress field of Italy. Throughout the Apenninic belt, an active extensional stress regime is observed. Compression stress regime is instead present along the Adriatic foredeep, with S_{Hmax} direction oriented N-S in the northern part and that rotates to NE-SW moving southward.

Source focal mechanisms recovered from on-line catalogs and from literature (EMMA database, VANNUCCI AND GASPERINI, 2003; 2004) have been used applying the seismic moment tensor summation technique (KOSTROV, 1974) to compute the seismic strain (Figure 1.4; VANNUCCI ET AL., 2004). Splitting the Italian peninsula in a regular grid with mesh of half a degree over which the sum of moment tensors is applied it is again found that along the chain and in the inner part of it the deformation is extensional while along the outer part the regime of deformation is mainly compressional.

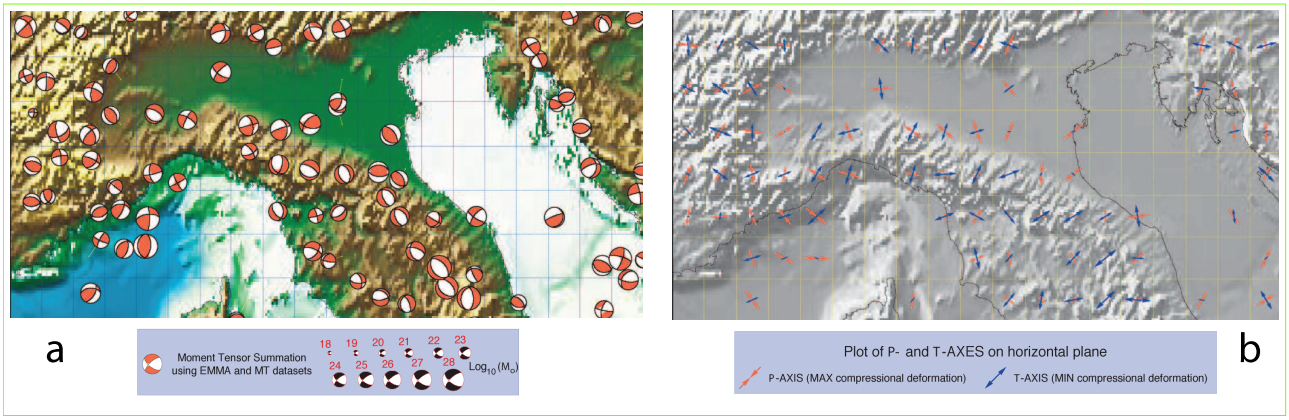

Figure 1.4: *a)* Sum of moment tensors from on-line catalogs (CMT, Regional CMT, ETH) and from literature (EMMA database) performed on a regular grid with mesh of half a degree, using earthquakes with depth < 50 km. The focal mechanism plots are scaled with magnitude and located in the center of mass of the epicenter distributions weighted with magnitude. *b)* Horizontal projections of P and T axes of cumulative tensor of plot a.

Recent geodetic results (SERPELLONI ET AL., 2005) calculated using continuous GPS measurements and local/regional GPS campaign, defines the rate of horizontal strain velocity. In a reference frame with fixed Eurasia plate, the extension is mainly confined in the Tuscany region, with NE-SW direction and a rate of 3.3 mm/yr. In the Po-Adriatic sector, the compression has a N-S direction with a rate of 0.8 mm/yr. The whole deformation rate for the Northern Apennines is therefore lower than 1 mm/yr,

lower respect to those in the southern part of the Apennines (1.6-5 mm/yr, SERPELLONI ET AL., 2005). In contrast, STEIN AND SELLA (2006) report that Adria and Apennines are not converging but they are moving toward NE together.

1.4 DEEP STRUCTURE BENEATH THE NORTHERN APENNINES

Many authors refer that the extension in the Apennines has been strongly associated with retreat of the subducting Adria slab (DEWEY, 1980; DOGLIONI, 1991; ROYDEN, 1993; MALINVERNO AND RYAN 1986; PINI, 1999; ZATTIN ET AL., 2002; PICCOTTI AND PAZZAGLIA, 2008). This subducting slab has been observed thanks to the several tomographic models produced in the last 15 years (WORTEL AND SPACKMAN, 1992; SPACKMAN ET AL., 1993; LUCENTE ET AL., 1999; PIROMALLO AND MORELLI, 2003). In particular, tomographic images of LUCENTE ET AL. (1999) and PIROMALLO AND MORELLI (2003) (Figure 1.5) evidenced the presence of an high velocity body running beneath the chain. This body is continuos between 250 and 670 Km, while in the shallower part it is more fragmented. LUCENTE ET AL. (1999) shows that the subducting body beneath Tuscany to Po-Plain region is very steep in the first 400 Km while moving deeper the dip decreases.

Studies of seismic refraction (PONZIANI ET AL., 1995), seismic reflection (MAKRIS ET AL., 1999) and CROP 3 line interpretations (BARCHI ET AL., 1998; MORGANTE ET AL., 1998) showed the presence beneath the Northern Apennines of two Mohos. The shallower one at 25 Km deep located in the south-western part of the region (Tuscany), and a second one located in north-eastern sector, with a depth between 30 to 50 Km depending on the different papers. The disparity of crustal thickness on the eastern and western flanks of the Apennines is a long-standing discussion. Moreover, observations show the highly complex nature of the crust on the Adriatic side of the orogen, and the uncertain position of the crust-mantle boundary. PAUSELLI ET AL. (2006) describe a reflection work on the CROP3 project, and show only short discontinuous reflections. To underline the certain complexity of the structure beneath the Adriatic side can be used the three studies done utilizing different versions of the Receiver Function technique. They have been done on a single data set from a short seismic deployment and obtained different conclusions on the thickness of the crust near the Adriatic coast (LEVIN ET AL., 2002; PIANA AGOSTINETTI ET AL., 2002; MELE ET AL., 2003) with values ranging between 30 Km on the Adriatic side to 40-50 Km beneath the Apenninic chain. On the contrary, simplicity and uniformity of Tuscan crustal structure has been described by interpreters of DSS studies (wide-angle reflection and refraction; PONZIANI ET AL., 1995). What is however demonstrated by all these papers is that the crust beneath Tuscany is thinner than beneath Adriatic side. These concepts are confirmed also by trench-retreat geodynamical reconstruction described by PICCOTTI AND PAZZAGLIA (2008).

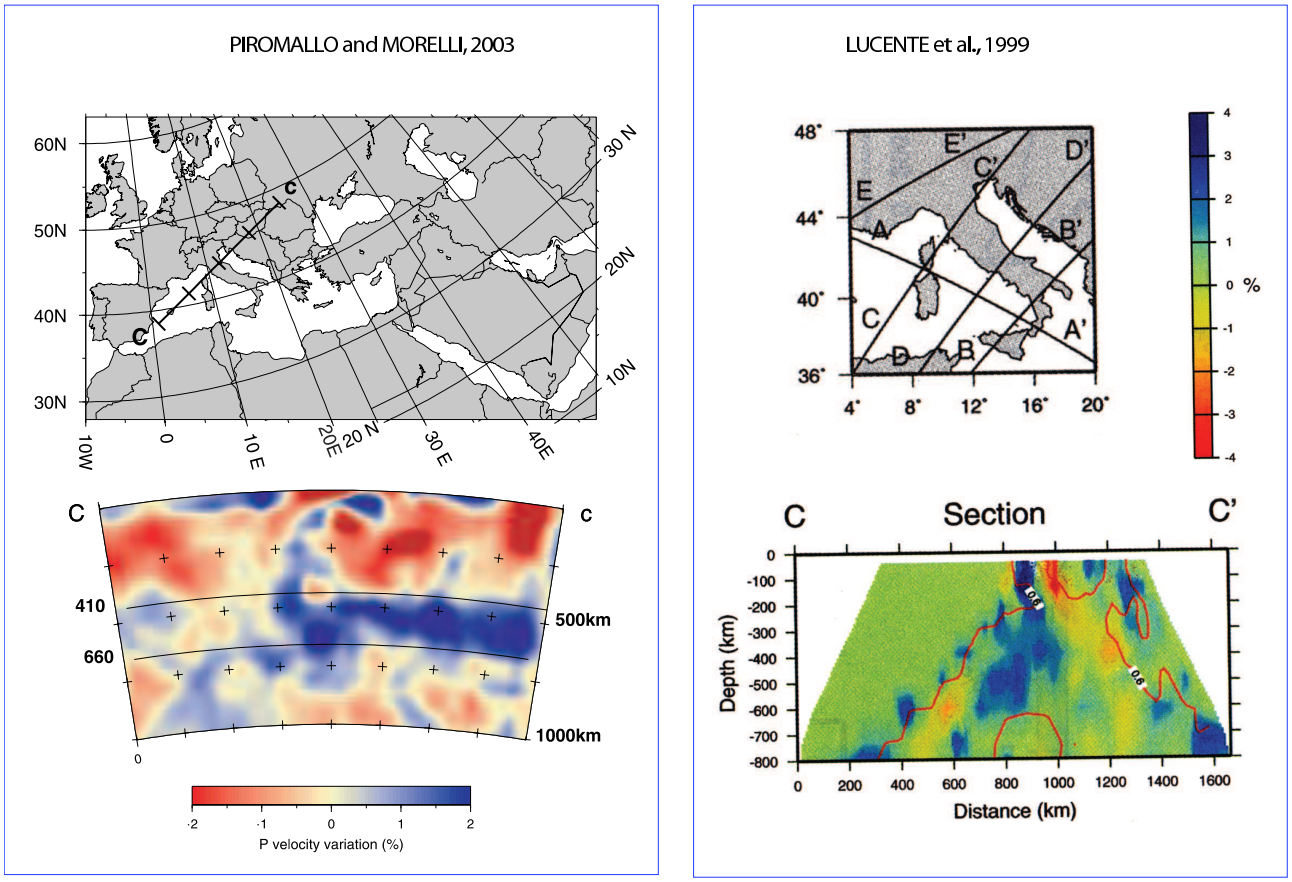

Figure 1.5: Tomography sections of the Northern Apennines.

Chapter 2

SHALLOW DEFORMATION

In this section we describe the research made to compute and interpret the shallow deformation gathered in Northern Apenninic area. With the term *shallow* we refer to deformation located in the crust, energy accumulated by tectonics forces during relative plates movements and relaxed in various form, first of all trough seismicity.

Several geophysical evidences can be helpful to image crustal deformation. Geodetic studies could give information about kinematics of continental deformation at plate boundaries, allowing us to derive the present day relative plates movements; structural geology can recover information about orientations of active faults and can recover information about deformations history at local scale; bore-hole breakout data from deep wells allow to constrain the direction of the minimum and maximum horizontal stress, giving information about regional state of stress and on the correlation between the active stress and tectonic structures. Given the high rate of low and moderate seismicity present in the area, we choose to analyze crustal deformation using seismological tools giving our attention to the study of seismic sources. In fact focal mechanisms studies provide essential information for mapping active tectonic regimes and seismic hazard (e.g., JACKSON AND MCKENZIE, 1988; ZOBACK, 1992; PONDRELLI ET AL., 1995; MONTONE ET AL., 1999, 2004; FAENZA ET AL., 2003; VANNUCCI ET AL., 2004). Added to geodetic data, that give information about aseismic deformation (and that themselves only determine the motion and velocities of crustal blocks), the ongoing deformation regimes can be imaged (SERPELLONI ET AL., 2005 and references therein). The most complete descriptions of a seismic source is made using seismic moment tensor representation that provides information about the relative movements of the rocky fault sides.

One of the most famous technique to calculate the seismic moment tensor is that built up by Harvard University and named Centroid Moment Tensor (CMT) (DZIEWONSKI ET AL., 1981). This technique,

developed with contributions of various authors in a time span of 20 years, allows to obtain seismic source parameters comparing recorded seismograms with synthetics one. Traditionally in the calculation are used body waves produced by large earthquakes ($Mw \geq 5.5$). Recently, ARVIDSSON AND EKSTRÖM (1998) have modified this procedure allowing the use of surface waves, more useful to determine seismic source parameters for earthquake with smaller magnitude ($Mw > 4.0$). With new seismic moment tensors computed with this last technique we determined the pattern of seismic deformation and active tectonic regimes in the Northern Apennines.

2.1 DATA DETERMINATION: SEISMIC MOMENT TENSOR, CMT AND RCMT

Every earthquake can be represented by source parameters. The hypocentral coordinates give information about the location of the fault while the seismic moment tensor components give information about the orientation of the fault and the motion which acted over it. With these information we have the complete representation of the earthquake source. In seismology communities the most appropriate model to simulate the behavior of an earthquakes follows the double-couple theory (Figure 2.1). This assumes that earthquakes are generated by shear faulting for which the equivalent force system in an isotropic medium is a pair of forces couples with no net torque (a double couple or DC). In practice, it summarizes the earthquake source mechanism as two couple of forces acting perpendicular and parallel to the fault. It's possible to define therefore two nodal planes over which the forces act. Every nodal plane is defined by two vectors oriented parallel (slip vector) and perpendicular (normal vector) to the fault and the definition of these parameters allow us to know the seismic moment tensor's component (Figure 2.1).

Due the importance that earthquake's information provide to various solid earth subjects, in the last 25 years several techniques have been elaborated to compute the source parameters. The most known is the Centroid Moment Tensor technique (DZIEWONSKI ET AL., 1981). This method allows to define the seismic moment tensor components comparing the observed and synthetics seismograms recovered with theoretical model of earth structure. The time window between P-wave arrival and the first arrival of fundamental mode surface waves, e.g. body waves, is compared. Using this part of seismograms and matching with syntethics computed in a three-dimensional Earth structure model, information about earthquakes with magnitude greater than 5.5 are obtained.

Using the terminology of GILBERT AND DZIEWONSKI (1975), a component of ground motion exited by a source point may be expressed by

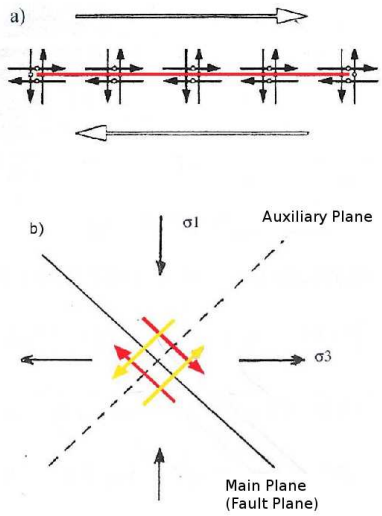

Figure 2.1: *a)* Plan view of a vertical strike-slip shear fault in a isotropic medium, showing the direction of slip (open arrows) and the equivalent distribution of double-couple force systems (solid arrows with forces applied at white dots). *b)* Distribution of principal stress axes along the main and auxiliary planes. The double-couple systems (red and yellow arrows) will act over both planes eluding the torque and net forces balancing.

$$u_k(r,t) = \sum_{i=1}^{6} \psi_{ik}\ (r,\, r_s,\, t\,) * f_i(t) \tag{2.1}$$

where u_k is the k-th record in the set of seismograms, r and r_s correspond to receiver and source location respectively. The functions $f_i(t)$ represents the six independent components of the moment tensor and are defined, in spherical coordinate system, as $f_1 = M_{rr}$, $f_2 = M_{\theta\theta}$, $f_3 = M_{\phi\phi}$, $f_4 = M_{r\theta}$, $f_5 = M_{r\phi}$, $f_6 = M_{\theta\phi}$. All these components are different to zero when a deep earthquake is analyzed while f_4 and f_5 become very small for very shallow sources (less than 5 Km) and become zero at the surface (DZIEWONSKI ET AL., 1981; ARVIDSSON AND EKSTRÖM, 1998). The ψ_{ik} represent the excitation kernels. They depend on the properties of the earth and are used to obtain the synthetics seismograms.

Assuming to know an initial estimate of the moment tensor f_0, we can define the differences between observed and synthetic seismograms as

$$u_k - u_k^0 = b_k \delta r_s + c_k \delta\theta_s + d_k \delta\phi_s + e_k \delta t_s \sum_{i=1}^{6} \psi_{ki}^0 * \delta f_i \tag{2.2}$$

where u_k^0 is the theoretical displacement calculated for the starting source coordinates and the initial estimate of the moment tensor, and b_k, c_k, d_k and e_k are the kernel functions defined as

$$b_k(t) = \sum_{i=1}^{6} \frac{\delta\psi_{ki}^0}{\delta r_s} * f_i^0 \tag{2.3}$$

$$c_k(t) = \sum_{i=1}^{6} \frac{\delta\psi_{ki}^0}{\delta \theta_s} * f_i^0$$

$$d_k(t) = \sum_{i=1}^{6} \frac{\delta\psi_{ki}^0}{\delta \phi_s} * f_i^0$$

$$e_k(t) = -\sum_{i=1}^{6} \frac{\delta\psi_{ki}^0}{\delta t} * f_i^0$$

The small perturbations in the source coordinates and origin time (δr_s, $\delta\theta_s$, $\delta\phi_s$, δt_s) and those in the moment tensor components (δf_i) are determined. These estimates allow to define new source parameters and new moment tensor's elements, that will become new input for an iterative procedure that, at the end, allows us to obtain the best fit between synthetic and real seismograms. The results will be the coordinates of the centroid (the center of mass of the rupture), the elements of the seismic moment tensor.

Following this technique, the Centroid Moment Tensor (CMT) Catalog (DZIEWONSKI ET AL., 1981; EKSTRÖM ET AL., 2005) was built up. It lists solutions for events worldwide with $Mw > 5.5$ and from 1977 to the present. CMTs have shown to be robust, stable, and reliable determinations of seismic source mechanisms. Traditionally for this calculation are used the body wave.

A recent evolution of the standard CMT method allows to use also surface waves and to analyze events with lower magnitude (ARVIDSSON AND EKSTRÖM, 1998). Thanks to this new opportunity, since 1997, a regional extension of the global CMT data set is compiled by the INGV (Istituto Nazionale di Geofisica e Vulcanologia) for all events with a moderate magnitude for the Mediterranean region. The European-Mediterranean Regional CMT (RCMT) Catalog lists about 600 solutions for earthquakes with $4.5 < Mw < 5.5$, occurred between 1997 to 2004 for the whole Mediterranean (PONDRELLI ET AL., 2002; 2004a; 2007).

2.1.1 THE UPDATE OF THE EUROPEAN-MEDITERRANEAN RCMT CATALOG IN THE ITALIAN REGION: THE ITALIAN CMT DATASET

The Regional Centroid Moment Tensors becomes an important seismological tools in those regions where a moderate seismicity occurs, as for example the Italian peninsula. The CMT catalog contains solutions for worldwide earthquakes with $Mw \geq 5.5$ from 1977 to now. The European-Maditerranean Regional CMT Catalog contains instead solution for earthquakes occurred in the Mediterranean region from 1997 up to now. Therefore between these two catalogs exists an inconsistency of about 20 years of data,

from 1977 to 1996. To resolve it at least for the Italian region, solutions for earthquakes occurred between 1977 and 1996 have been calculated (PONDRELLI ET AL., 2006). We selected earthquakes from 1977 to 1996, with a bulletin magnitude between 4.7 and 5.5, located in the extended Italian region with latitude between 36°N and 48°N, and longitude from 6°E to 20°E for which a CMT solution was unavailable. This preliminary dataset includes 148 candidate events. Hypocentral data and magnitudes are recovered from the catalog of the USGS National Earthquake Information Center (*http://wwwneic.cr.usgs.gov/neis/epic/*). In some cases also those from the bulletin of Istituto Nazionale di Geofisica e Vulcanologia (*http://waves.ingv.it*) are used. Long period waveforms for all these earthquakes were retrieved from the IRIS Data Management Center (*www.iris.edu*).

Although only stations located at regional distance are usually used in the calculation of RCMTs for current seismicity, in this work, when closer stations alone were insufficient for a stable inversion, for several events occured before 1990 we also used stations at teleseismic distances. This procedure has shown to produce good quality synthetic seismograms and likely moment tensor solutions (Figure 2.2; see also PONDRELLI ET AL., 1999; 2001).

To maintain a consistency with other European-Mediterranean RCMTs, we apply to the new solutions the same quality criteria used for the Catalog (PONDRELLI ET AL., 2002). In critical areas, with scarce seismicity, we choose to relax the quality criteria not to discard earthquakes holding a special interest because of their location. However, we track solution reliability by using a quality flag (Table 1 in PONDRELLI ET AL., 2006): A flag identifies full compliance to all quality criteria, while following letters (up to D) correspond to decreasing levels of quality. B flag is given to those moment tensors that have a difference between preliminary and final coordinates, δ_{epic}, greater than 0.3°and lower than 0.5°. If $\delta_{epic} \geq 0.5°$the coordinates are kept fixed along the inversions and the flag becomes C. Usually these coordinates variations are due to a low quality in the azimuthal distribution of stations. Flag D is given only when the resulting moment tensor has a high non-double couple component due to low signal-to-noise ratio. Changes in δ_{epic} and a large non-double-couple component can be considered indicators of a complex seismic source but for large magnitude events only. On the contrary, for moderate magnitude earthquakes, such as those studied here, they are commonly related to low quality of seismographic data. Introducing the use of quality factors, about 20% more events could be retrieved. The quality flag frequency distribution results in 77% in A class, 12% in B class, 3% in C class and 8% in D class. All together, we determined RCMTs for 65 earthquakes. The computed source parameters (PONDRELLI ET AL., 2006) are mapped in yellows in Figure 2.3.

We also matched our new moment tensors with data from the EMMA Database (VANNUCCI AND GASPERINI, 2003; 2004) by computing the angles between P and T axes as well as the angle between the dihedrals (couples of planes) representing best double-couples of focal solutions common to both

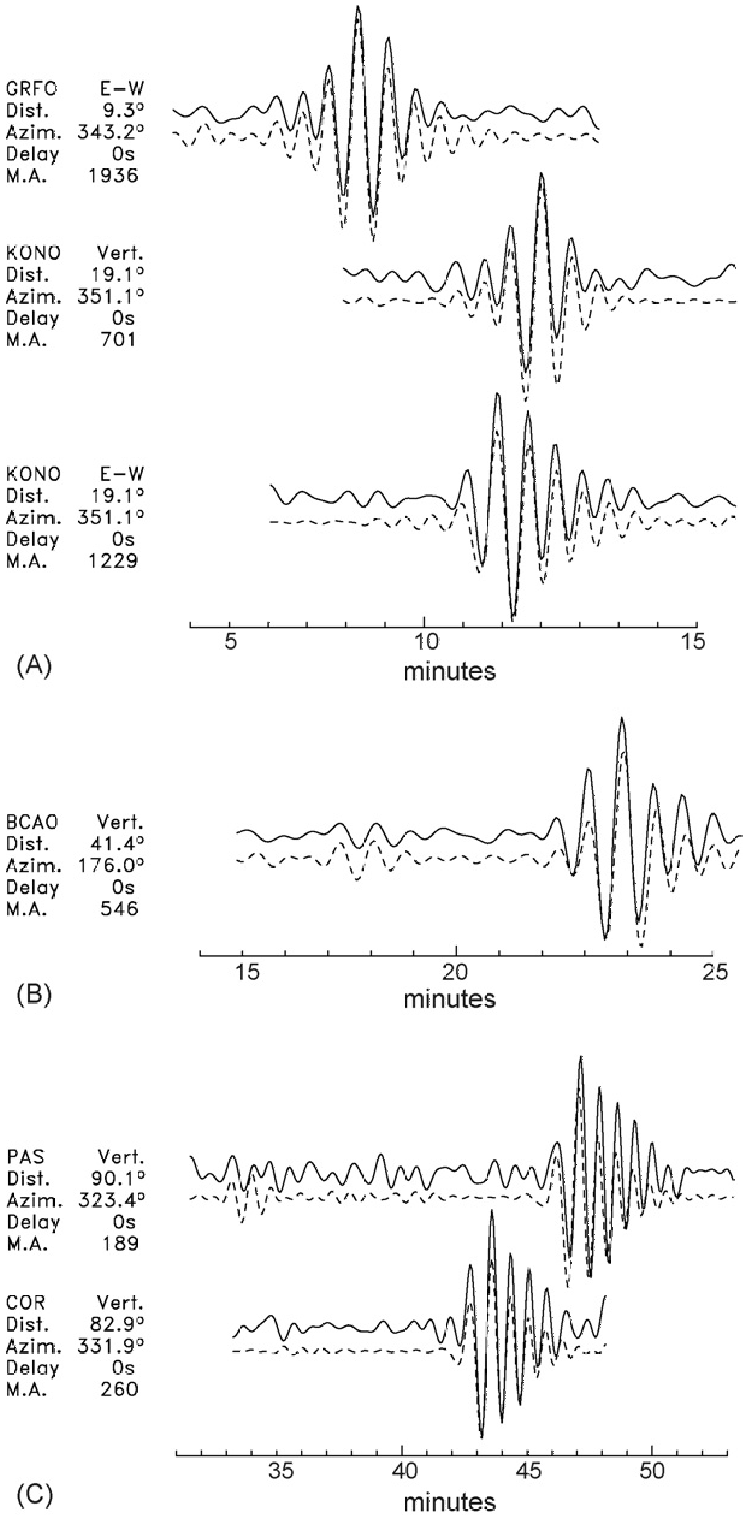

Figure 2.2: Data (black line) and synthetic (dotted line) seismograms. Panel A: example of comparison for stations at regional distance; panels B and C: example of comparison for stations at greater distances.

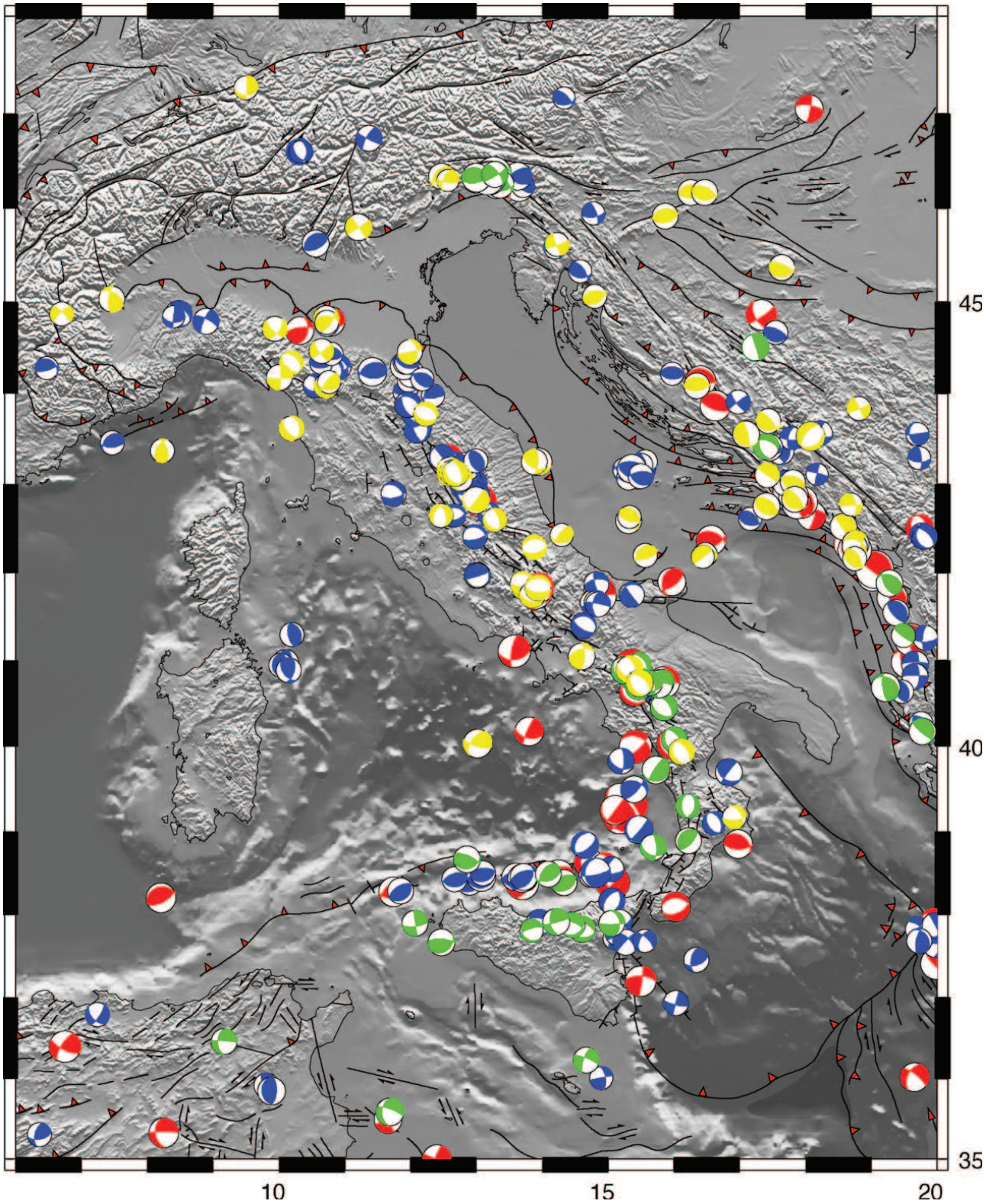

Figure 2.3: Map of all moment tensor solutions included in the Italian CMT dataset. Harvard CMT Catalog solutions are in red, European Mediterranean RCMT solutions are in blue, RCMT from previous papers are in green and new RCMTs from this work are in yellow.

datasets (Figure 2.4). Following KAGAN (1991), the Kagan angle (Figure 2.4) measures the rotation that should be applied to one double-couple to make it coincident with another one. It may vary from 0°(perfect agreement) to 120°(total disagreement), thus values well below 60°indicate a good correspondence while above 60°a mismatch. The comparison has been possible for 30, without class distinction. For about 50% of them the difference is well above 60°indicating a strong mismatch. However, several focal mechanisms computed after the nineties (e.g., data from FREPOLI AND AMATO, 1997, 2000; EVA AND SOLARINO, 1998; SUE ET AL., 1999) are mostly similar to ours. For instance, the two events S101095A and S123195A, occurred in the Northern Apennines, show the same strike-slip focal mechanism from waveform modeling and from P first arrival determination (FREPOLI AND AMATO, 1997). However, also extreme examples exist, such as for events S042688A and S012686A, for which the angle between the first pulse solution and ours almost reaches the maximum value 120°, corresponding to a circular swap of the three major axes: P to T, T to N and N to P. That behaviour cannot be attributed only to experimental uncertainties, but is likely due to wrong estimates of polarities. Older fault plane solutions, based on first motion polarities, show therefore to be affected by large uncertainty, possibly due to the intrinsic large sensitivity of the method to a single or few wrong reports when data are scarce.

We merge the new RCMTs with global CMT and European-Mediterranean RCMT catalogs for the Italian region, to obtain a comprehensive dataset dating back from 1977, and representing more than 25 years of seismic activity (Figure 2.3). Altogether the dataset lists 338 centroid moment tensors, for shallow and intermediate depth earthquakes, and magnitude between 4.0 and 6.9. Sixty solutions come from the Harvard CMT Catalog, 170 from the European-Mediterranean Catalog, 43 from previous papers (PONDRELLI ET AL., 1999, 2001, 2004b; CUCCI ET AL., 2004) and 65 from this study (in yellows; PONDRELLI ET AL., 2006). All data included in this Italian dataset are available on the web at the address *http://www.bo.ingv.it/RCMT/Italydataset*, where all technical characteristics for each moment tensor solution, as the number of used stations and low period cut-off are described.

Solutions for some of the earthquakes studied here also appear on the Harvard CMT Catalog, mainly events occured after 1997. Surface waves at regional distance have a better signal-to-noise ratio than long period body waves at global distance, and the RCMT method appears more appropriate in modeling smaller magnitude seismic sources. Therefore, when both solutions exist for an earthquake, we choose the RCMT when $Mw \leq 5.5$, and the CMT solution otherwise. All RCMTs represent only a small fraction of the total released seismic moment, the largest part of which is represented by greater-magnitude events included in the Harvard CMT Catalog. The new events, however, greatly improve the characterization of some areas and the reduction of the magnitude completeness threshold for the dataset.

ID	References	Kagan Angle	P Axes difference	T Axes difference	NEW DATA	EMMA DATA
S073078A	Gasparini et al., 1985	87.61	87.00	87.56		
S120578A	Gasparini et al., 1985	37.12	28.00	26.99		
S041779A	Muço, 1994	81.98	73.99	30.44		
S051279A	Muço, 1994	54.36	20.64	52.22		
S010580A	Eva et al., 1997	27.92	27.65	26.45		
S022880A	Gasparini et al., 1985	75.50	32.36	68.58		
S060780A	Eva and Pastore, 1993	40.04	39.70	7.63		
	Eva and Solarino, 1992	76.87	71.11	50.15		
S110780A	Muço, 1994	82.50	32.37	78.22		
S122380A	Eva and Solarino, 1992	42.62	38.11	18.37		
S042281A	Nicolas et al., 1990	49.30	20.24	49.24		
	Eva and Solarino, 1998	74.10	26.53	68.07		
	Augliera et al., 1994	78.49	11.91	79.36		
	Baroux et al., 2001	48.99	11.91	49.00		
S112585A	Muço, 1994	92.68	70.81	68.91		
S010886A	Renner and Slejko, 1994	97.32	77.31	81.90		
S012686A	Renner and Slejko, 1994	106.75	70.83	82.72		
S082986A	Renner and Slejko, 1986	73.61	19.14	70.20		
S100186A	Eva and Solarino, 1992	66.43	42.97	49.58		
S122486A	Herak et al., 1995	56.12	51.74	21.39		
S042688B	Renner and Slejko, 1994	111.15	87.75	83.25		
S091389B	Eva and Pastore, 1993	8.13	6.70	5.00		
S012490A	Frepoli and Amato, 2000	26.29	25.14	7.64		
S090390A	Herak et al., 1995	98.87	64.37	66.00		
S021191A	Delacou et al., 2004	43.39	41.29	13.00		
	Sue et al., 1999	34.21	31.39	13.00		
S090891A	Herak et al., 1995	13.40	13.31	13.30		
S071692A	Frepoli and Amato, 2000	47.12	18.98	46.67		
S060193A	Herak et al., 1995	47.37	19.99	42.73		
S060593A	Frepoli and Amato, 1997	75.59	46.80	65.69		
S052295A	Herak et al., 1995	40.60	17.74	36.37		
S082495A	Frepoli and Amato, 1997	55.35	47.69	27.11		
S101095A	Frepoli and Amato, 1997	16.46	15.62	11.94		
S123195A	Frepoli and Amato, 1997	16.04	11.90	12.78		
S122196A	Selvaggi, 2001	40.89	20.42	40.62		

Figure 2.4: Sketch of comparison between new solutions from the Italian CMT dataset and P first polarities solutions included in EMMA Database (VANNUCCI AND GASPERINI, 2003; 2004). The Kagan angle (see text), the difference between T and P axes of the two focal solutions are shown.

2.2 SEISMIC DEFORMATION THROUGH MOMENT TENSOR SUMMATION

To have information about seismic deformation in the study region, we apply the moment tensor summation method (KOSTROV, 1974). Summing all moment tensors of earthquakes occurred in a given volume, a cumulative moment tensor that summarizes the seismic deformation is computed (MOLNAR, 1983; JACKSON AND MCKENZIE, 1988; EKSTRÖM AND ENGLAND, 1989; PONDRELLI ET AL., 1995).

Inside a given volume V the average strain $\overline{\varepsilon}_{ij}$ could be relate to earthquake moment tensor by

$$\overline{\varepsilon}_{ij} = \frac{1}{2\mu V} \sum_{k=1}^{K} M_{ij}^{k} \tag{2.4}$$

where M_{ij}^{k} is the ij-th component of the moment tensor M_{ij}, V the interested volume and μ the shear modulus. The average strain rate, i.e parameter defining the variation of $\overline{\varepsilon}_{ij}$ in a time length τ, could be calculated by

$$\widehat{\varepsilon}_{ij} = \frac{\overline{\varepsilon}_{ij}}{\tau} \tag{2.5}$$

The tectonic regimes resulting from a moment tensor summation can be displayed by a color representation of the FROHLICH (1992, 2001) ternary diagram, where red corresponds to a purely compressive regime, green to a strike-slip regimes and blue to purely extensional regime. Composite colors indicate mixed tectonic regimes. The principal seismic strain directions can also be mapped as horizontal projections of maximum compression (P) and traction (T) axes of the cumulative moment tensor in each cell.

The method described above was applied to the entire Italian peninsula, from 6°E to 20°E of longitude and between 36°E to 43°E of latitude. This area was splitted in cells of 0.25°x 0.25°inside which the moment tensor summation method was applied. Here we describe what has been achieved for the Northern Apennines. Accordingly with previous publications on this subject (i.e PONDRELLI ET AL., 1995) the shear modulus value used is $3 * 10^{-12} Nm^{-2}$. The data used are all CMTs and RCMTs (the Italian CMT dataset) adding the data from EMMA database (VANNUCCI AND GASPERINI, 2003; 2004), that contains focal mechanism recovered from literature.

2.3 DISCUSSION ON SHALLOW DEFORMATION RESULTS

The importance of RCMTs and of the compilation of the Italian CMT dataset (Figure 2.3; PONDRELLI ET AL., 2006) can be mainly found in the increase of data available for seismotectonic studies. Indeed,

data included in this catalog are important to characterize the active tectonic, mainly where seismicity of moderate magnitude, as in our study region, prevails. Here, the contribution of new mechanisms confirms the presence of extensional styles in the eastern part of the Apennine (Figure 2.5). Some new mechanisms indicate also a prevailing strike-slip style in some areas previously not well documented like the northernmost part of the Apennines, the central to southern Po plain and the Garfagnana-Lunigiana area. All available moment tensors for events located along the outer part of the chain, show prevailing strike-slip to thrust solutions, with P axes always in a NE-SW direction. On the contrary, extensional focal mechanisms, with T axes perpendicular to the belt strike, are mostly in the inner part of the chain, on the Tuscany side (Figure 2.5). The divide (orange line in Figure 2.5) separates quite strictly the parts where the two different type of mechanisms are distributed. Moreover, if we take into account the distribution at depth of these different mechanisms, it can be noted that strike-slip and thrust events have deeper hypocentral location, often between 20 and 30 km (grey background focal mechanisms of Figure 2.5) respect to extensional events, generally located within the first 10 km of depth. Another feature that here we can underline is the presence of prevalent strike-slip mechanisms in the northernmost part of the Apennines and around the northern buried thrusts below the Po Plain. These arcuate structures are the outermost part of Northern Apennines. Their shapes probably promote strike-slip motions due to the prevailing NE-SW trending compression applied on the several tectonic structures striking perpendicular to the chain (Figure 2.5). Pure thrust mechanisms, on the contrary, seem to prevail mainly in the rest of outer chain, south of 44.5°N, where thrust structures are more linear and parallel to the chain.

Joining these new moment tensors with focal mechanisms included in the EMMA database (VANNUCCI AND GASPERINI, 2003; 2004) and those from on-line catalogs (RCMT, CMT and other) we are able to define the seismic deformation pattern for a given region. We have split the Northern Apennines area in a grid with a 0.25°meshing and we applied the KOSTROV (1974) method inside each cell. In Figure 2.6 the obtained cumulative moment tensor is mapped, scaled as a function of the cumulative magnitude and calculated for a depth range from 0 to 800 Km.

Normal mechanisms are mainly distributed along the chain and in agreement with several extensional structures oriented in Apenninic direction. Inverse deformation dominates along the outer part of the belt (close to Adriatic Sea) and in the Po-plain area (close to 44°of lat), even if with a non-homogeneous orientation. A strike-slip deformation is more frequent in central Tuscany and along the north-western part of the Apennines.

Other information can be recovered splitting the map in two layers of different depths: the first describes 15 Km of depth (Figure 2.7a) and the second represent the interval from 15 to 40 Km of depth (Figure 2.7b). The normal and the strike-slip deformation present in Tuscany are constrained in the shallower part of the crust, i.e. in the first 15 Km (Figure 2.7a). Only a small portion occurs below this

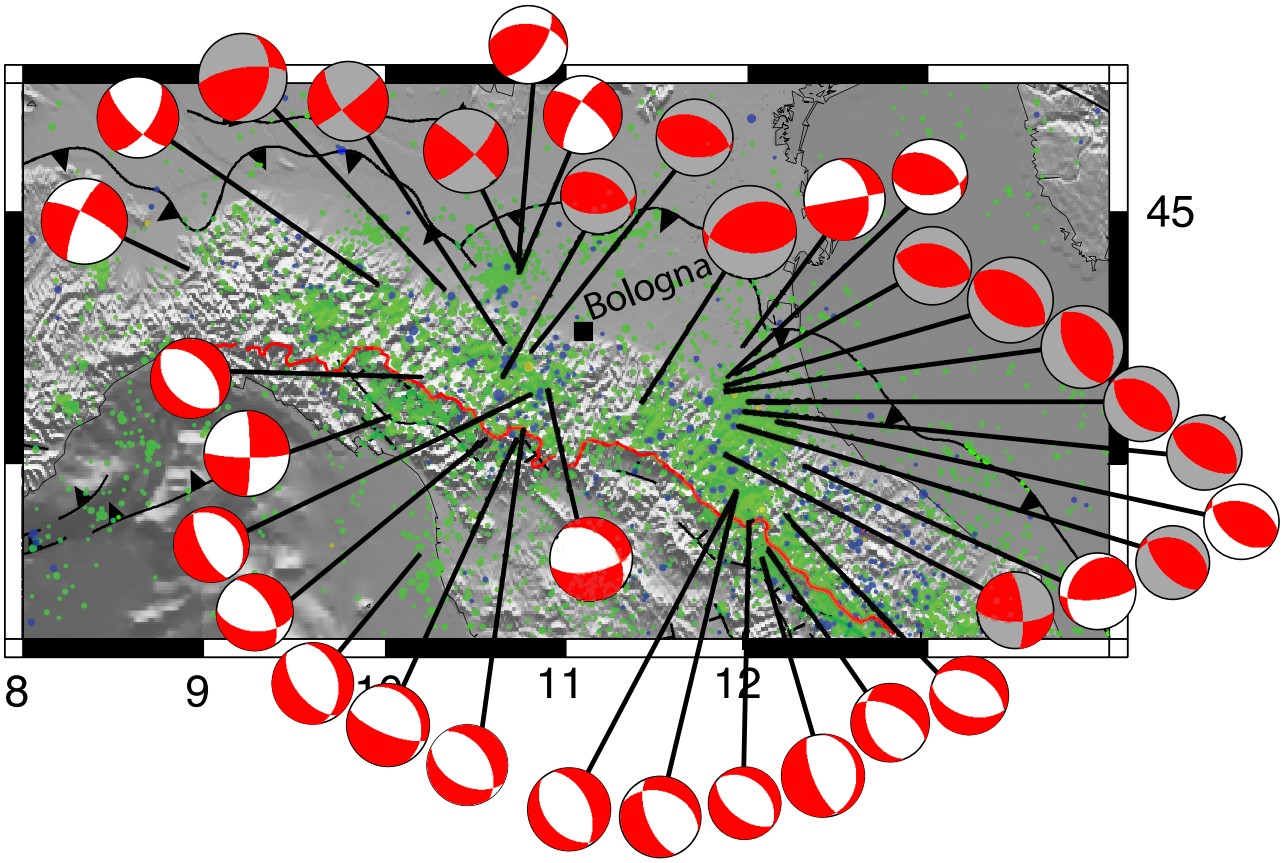

Figure 2.5: Seismic activity from the Italian national catalog (available at *http://www.ingv.it/CSI/*) mapped by dots color-coded by hypocentral depth: green, above 30 km; blue, between 30 and 100 km; and yellow, deeper then 100 km. Focal mechanisms are from Italian CMT data set (available at *http://www.bo.ingv.it/RCMT/Italydataset*) (PONDRELLI ET AL.,2006). They are shaded according to source depth: white background, above 20 km; and grey background, deeper than 20 km.

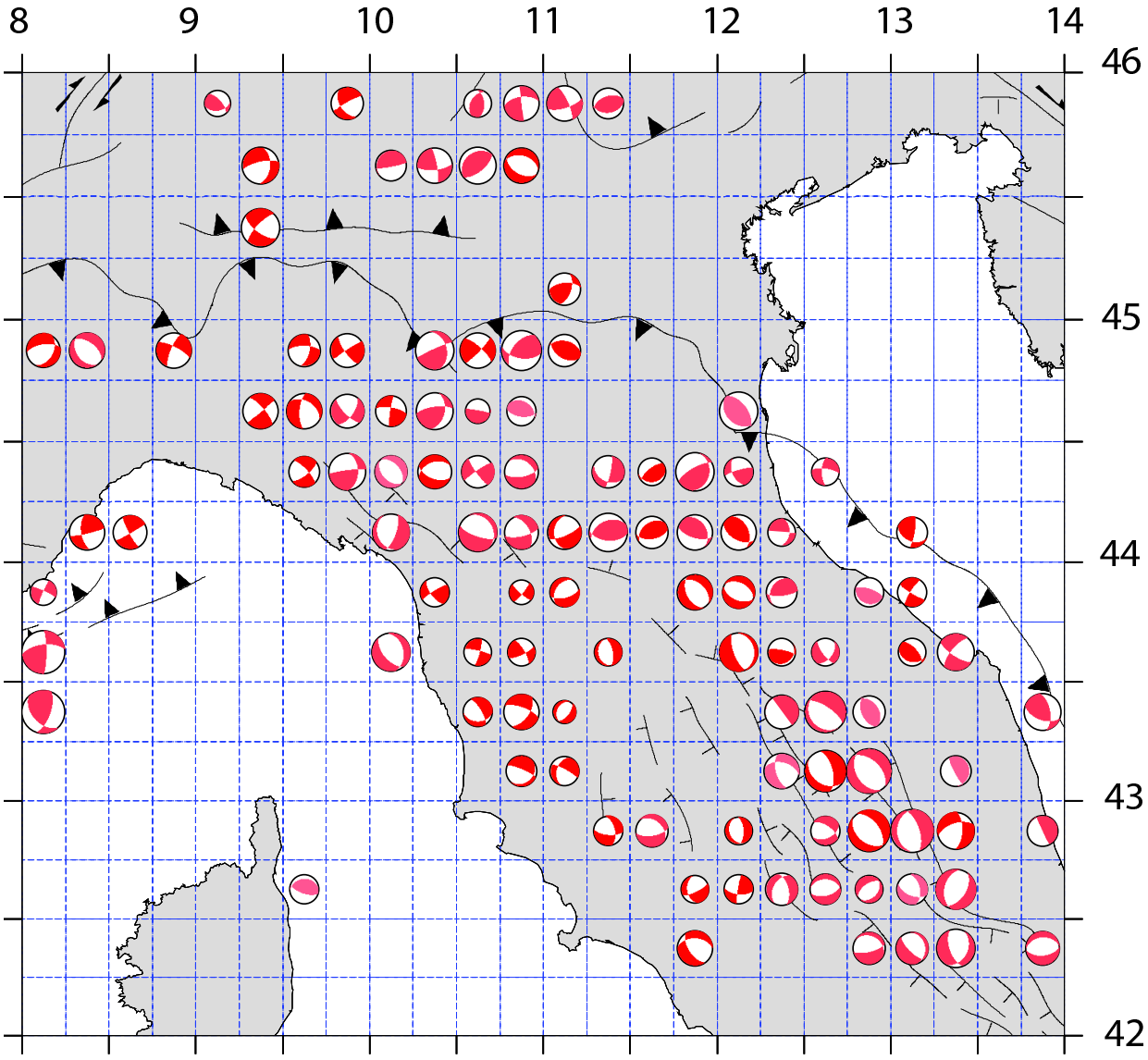

Figure 2.6: Map of the cumulative moment tensor calculated from literature data and on-line catalogs in a depth range between 0 to 800 Km. The grid used has a 0.25°meshing. Mechanism are scaled with the magnitude and different red gradients correspond to a different cumulative depth.

depth and it is mainly located in the north-western part of the Northern Apennines (Figure 2.7b). The distribution of the T axes (in blue in Figure 2.8) emphasizes as in the shallower part, a clear rotation from NE-SW to N-S occurs moving northward. The continuity of this rotation is broken by locally NW-SE directions that become less evident beneath Tuscany region. At greater depth, the T-axes orientation are NE-SW and NNE-SSW for most of measurements.

The compressive deformation instead occurs both in the shallower and in the deeper part. Altought the mechanism remains compressive the orientation changes above and below 15 Km of depth showing the different behavior of seismic sources. This is verified also observing the P-axes orientation (in red in Figure 2.8). Between 15 and 40 Km the P-axes are mainly concentrated in the outer part of the chain with NNE-SSW orientation, that becomes N-S and NW-SE moving toward NW. NE-SW azimuth is also the most frequent direction for the outer part of the belt above 15 Km, but also E-W and NNW-SSE directions occur in some cells.

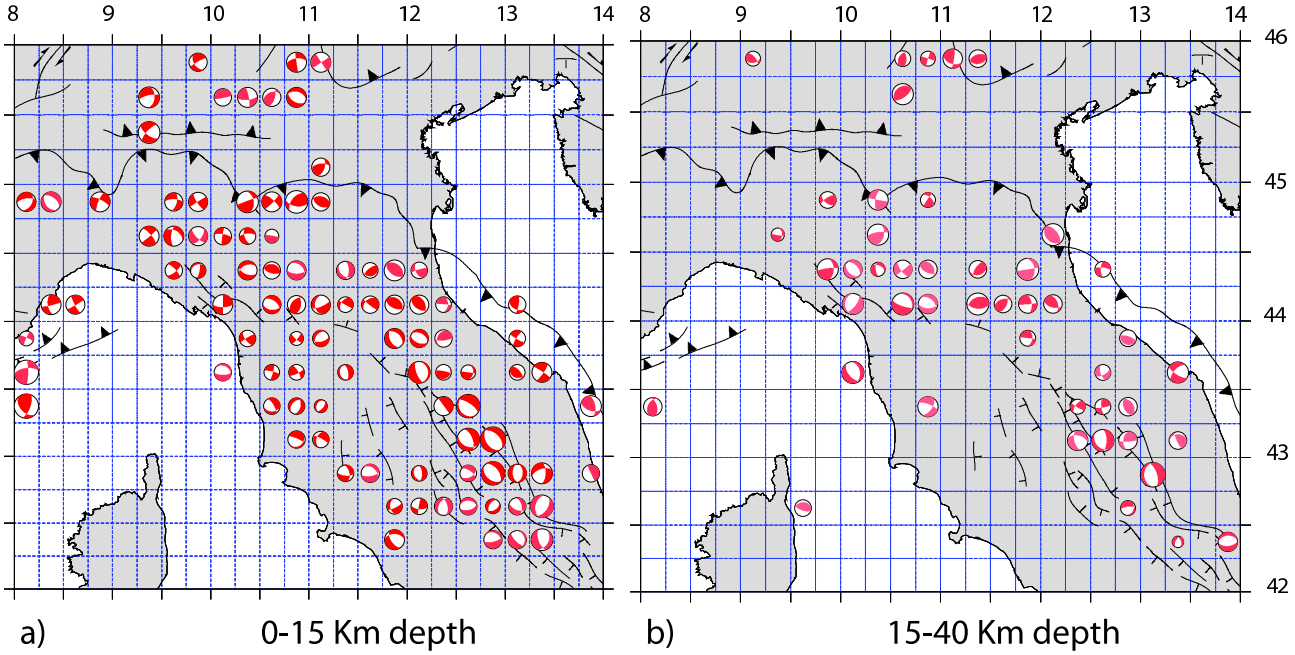

Figure 2.7: Cumulative moment tensors as a function of depth. *a)* from 0 to 15 Km of depth and *b)* from 15 to 40 Km of depth.

An alternative seismic strain representation is given by the Frohlich ternary diagram (FROHLICH, 1992; 2001) that allows to define from a focal mechanism a tectonic regime. As shown in the inset of Figure 2.9, we associated the blue color to the extensional mechanisms, the red for inverse and the green for strike-slip mechanisms. Mixed behaviors are associated with a gradient of these three main colors.

We applied this representation to each cumulative moment tensor calculated for each cell and the

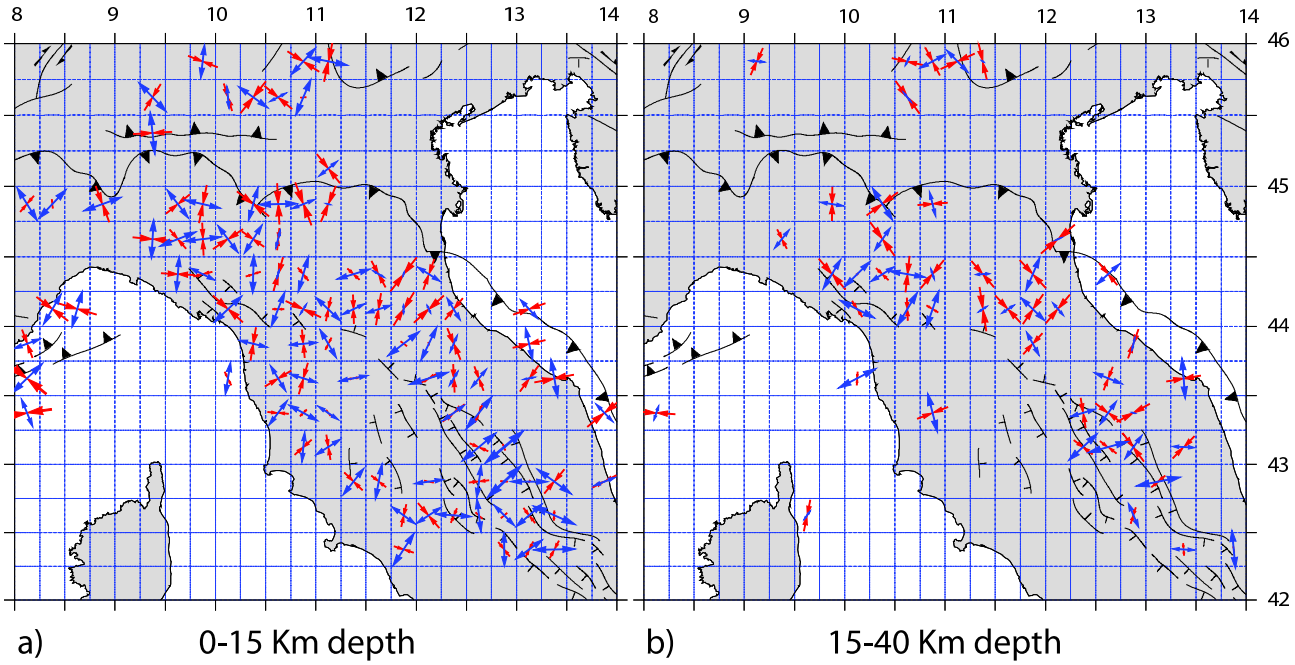

Figure 2.8: Distribution of P (in red) and T (in blue) axes of the cumulative moment tensors. *a)* from 0 to 15 Km of depth and *b)* from 15 to 40 Km of depth.

results are in Figure 2.9. In particular it is evident as the blue color is concentrated along the southern part of the study region and in Tuscany. Most of this kind of deformation is in the first 15 km depth (Figure 2.9b) while only in the northwestern part of Tuscany and in Central Apennines remains also at greater depth (Figure 2.9c). The strike-slip deformation is mainly concentrated on the west of the study region, but it occurs also along the Adriatic region together with compressive one (Figure 2.9a). Also the strike-slip deformation disappears below 15 Km of depth altought in some point in the chain and beneath the Po-Plain area remains. The compressive deformation occurs in the outer part of the chain in the first 15 Km of depth (Figure 2.9b) then, below 15 Km migrates beneath the crest of the chain (Figure 2.9c).

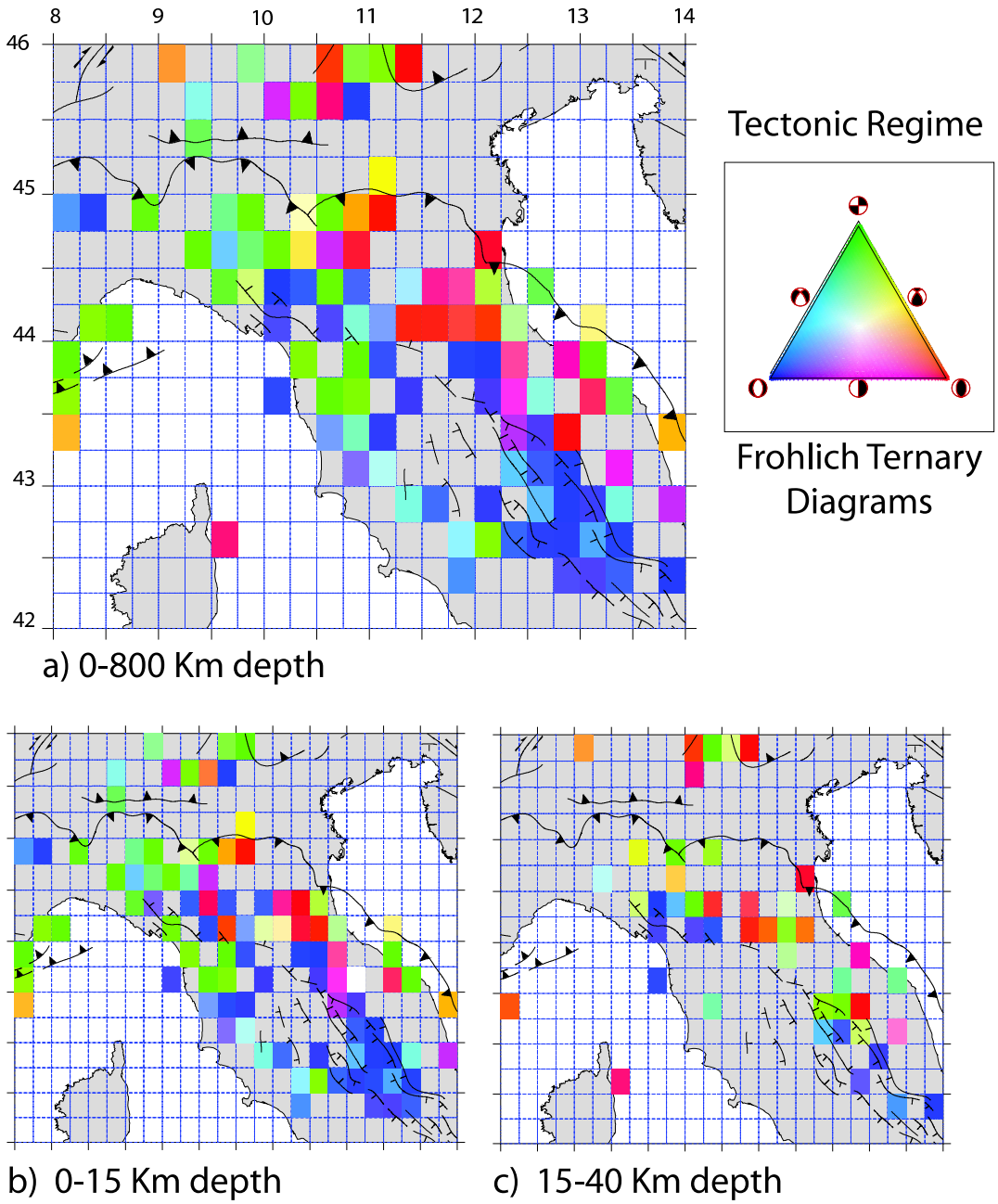

Figure 2.9: Tectonic regimes obtained from the sum of moment tensors applying the Frohlich ternary diagram methodology (FROHLICH 1992, 2001) for *a)* depth from 0 to 800 Km, *b)* depth from 0 to 15 Km and *c)* depth from 15 to 40 Km. The inset indicate which color is associated with normal, inverse or strike-slip earthquakes behavior.

Chapter 3

DEFORMATION AT DEPTH - MANTLE DEFORMATION

3.1 SEISMIC ANISOTROPY

After investigating the shallow deformation i.e, the deformation occurring mainly in the crust, the second goal of this study is to look into greater depths inside the upper mantle. The information regarding the mantle strain are recovered also in this case by seismological studies.

One of the most helpful seismological properties is the anisotropy. A medium whose elastic properties are functions of orientations is described as anisotropic (SILVER, 1996). A seismic wave crossing an anisotropic medium travels at different velocities, depending on its propagation direction and on its polarization direction. In the crust the anisotropy is due to the presence of aligned fluid filled cracks or alternating isotropic layers with different elastic properties; in the mantle the most important cause of seismic anisotropy is the lattice preferred orientations (LPO) of the mantle minerals. In the mantle, olivine is the main constituent and its crystals are intrinsically anisotropic (BEN ISMAIL AND MAINPRICE, 1998; SAVAGE 1999). This highly anisotropic component therefore tends to align its fast crystallographic axes (a-axis) parallel to astenospheric flow as a response to finite strain induced by geodynamic processes (SILVER, 1996).

There are several deformation processes that could take place in the mantle. The main types are diffusion and dislocation creep. The diffusion creep is a solid-state diffusion between grain boundaries or across the crystal lattice (KARATO AND WU, 1993). This mechanism acts at relatively low stress, small grain boundaries conditions and it doesn't produce LPO of mantle's mineral and therefore the deformed material is isotropic (KARATO AND WU, 1993). The dislocation creep instead acts as motion of crystalline

dislocations within the grains. It occurs at high stress, large grain size conditions and it causes the lattice preferred orientations in the upper mantle (KARATO, 1987; KARATO AND WU, 1993).

Various parameters besides the stress level and the grain boundary size influence the anisotropy. First, the type and magnitude of strain. In the case of progressive simple shear, for large strains, deformation's effect are reinforced by dynamic re-crystallization and the maximum strain is expected to align parallel to asthenospheric flow (olivine a-axes align within the foliation plane and nearly parallel to lineation's direction; RIBE, 1989; WENK ET AL., 1989). Anisotropy for olivine crystals under small strain condition, deformed in simple shear, yields the orientations of olivine a-axes parallel to the minimum principal stress (45°to the flow plane; ZHANG AND KARATO, 1995). Other factors are temperature and pressure. Higher temperature and pressure conditions support the generation of dislocation creep. The re-orientation of mantle minerals can be generated at temperature greater than 900°C. The presence of partial melt or scarce amount of olivine crystals in the bulk composition, instead, are factors that inhibit the action of dislocation creep, reducing the amount of the anisotropy in the rocks.

The source of anisotropy is mainly linked with deformation, mainly in the tectonically active areas. It can be observed in different ways. The most straightforward manifestations occur when measurements of wave speed provide different results for different azimuth. This is the case of *azimuthal anisotropy* (SAVAGE, 1999) and it could be studied by Pn tomography or examining the surface wave anisotropy. When phases with different polarization travel with different speed in an anisotropic medium we are in the case of *polarization anisotropy* (SAVAGE, 1999). Several studies allow to gain informations about it as for examples:

1) the surface wave scattering from Love (horizontally polarized shear) to Rayleigh (hybrid shear and compression): measured along different azimuth and for long periods ($>$ 70 s) can give strong evidence for lateral gradients in velocity (at 100 to 300 Km depth) (YU AND PARK, 1993).

2) the global average travel time of SH that are faster than SV (SHEARER, 1991; EARLE AND SHEARER, 1994)

3) shear wave splitting (VINNIK ET AL.,1984; SILVER AND CHAN, 1988; SAVAGE, 1999) that is the seismological analogous to optical birefringence.

The distinction between azimuthal and polarization anisotropy is very important. The first, comparing seismic waves traveling with different paths in the case of heterogeneous isotropic structures, undergoes lateral trade-off and generates path-dependent velocity variations. This trade-off is weaker in the case of surface waves and absent in the case of shear wave splitting. Therefore, compared to azimuthal anisotropy, the polarization anisotropy is less sensitive to heterogeneous isotropic structures and the interpretations of its measurements are more straightforward. For this reason we studied mantle deformation looking at polarization anisotropy by shear wave splitting analysis.

3.2 SHEAR WAVE SPLITTING

The shear wave splitting is a physical phenomenon similar to the birefringence in optical studies. In an isotropic elastic solid two types of elastic waves propagate (Figure 3.1): compressional or P-waves and shear or S-waves. Isotropic propagation therefore has linear P wave particle motion parallel to the propagation direction and S wave particle motion perpendicular to propagation, with two components arbitrarily defined as oriented in the horizontal (SH) and in the vertical plane (SV). For any isotropic medium the P and SV phases are identified in the radial component of the seismograms while the SH is contained in the transverse one (perpendicular to the radial). The amplitude of the SH and SV components are functions of the polarization directions. In the isotropic case, both the particle motion of the P- and S-waves are linear.

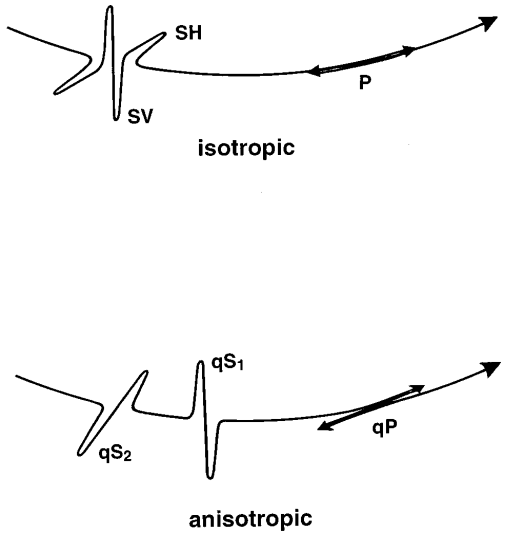

Figure 3.1: Three dimensional comparison of isotropic and anisotropic waves propagation (from SAVAGE, 1999 modified).

In a weakly anisotropic media, as in the Earth's crust and upper mantle, waves are neither purely longitudinal nor transverse to the direction of propagation. The P-wave velocity depends on the propagation direction while the S-wave velocity depends also on the polarization ones. Anisotropic propagation has therefore a quasi-P wave (qP in Figure 3.1) with linear particle motion that is not quite parallel to the propagation direction, and two quasi-S waves (qS1 and qS2 Figure 3.1) with polarization parallel and perpendicular to the fast direction.The term *quasi* is used because in most cases the polarization is about 10°from the parallel and perpendicular directions. So body waves crossing an anisotropic medium will generate a quasi P-wave and two quasi S-waves with different propagation's velocities. Typically the fastest shear wave is named quasi-S1 while the slower quasi-S2. In this case the particle motion of the

P-wave remains the same as the isotropic case, while that of S-wave changes turning into cruciform in the case of large splitting or elliptical in the case of small splitting (SAVAGE 1999). Besides the different polarization directions the two quasi-S waves arrive at different times due to difference in propagation velocity. This delay time (dt) is defined as

$$d_t = L(\frac{1}{V_{S1}} - \frac{1}{V_{S2}}) \tag{3.1}$$

where V_{S1} and V_{S2} are the speeds of the two quasi-shear waves (functions of the directions of wave polarization and material properties) and L is the length of the anisotropic path crossed. A shear wave traversing an anisotropic layer is split accordingly to equation 3.1. The phenomenon that generates the separation between the two components of S-wave is called shear wave splitting and the parameters that define it are the orientations of the anisotropic fast axis (ϕ) and the delay time (*dt*) between the arrival of the fast quasi S wave and the slow quasi S wave. The values of dt is linked with the thickness of the anisotropic layer crossed.

Various type of shear wave phases are used to recover shear wave splitting parameters in the mantle. The most frequently used is the SKS phase (Figure 3.2). It start as S-wave, passes through the fluid core as P-wave and converts again in an S-wave when passes through the receiver's mantle side. During the double S to P and P to S conversions, all the anisotropy previously accumulated, is erased and the anisotropy recorded by the phase is only that beneath the receiver. The other phases with similar behavior are PKS or SKKS.

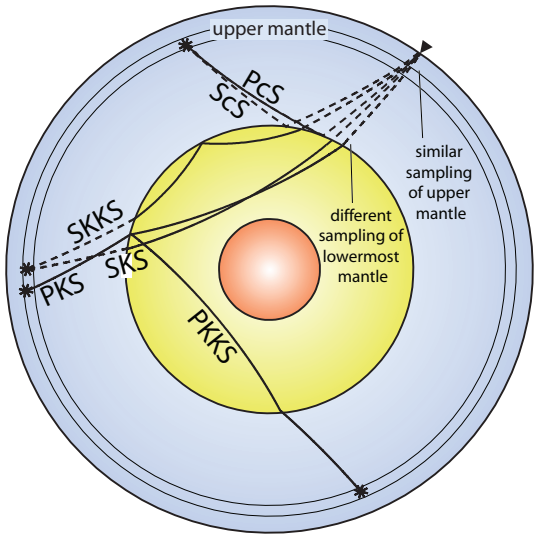

Figure 3.2: Various kind of body waves used in the seismic anisotropy analysis (from Garnero's web pages, *www.garnero.asu.edu*).

Another phase that can be analyzed is the S-wave. In this case, anisotropy is accumulated during the

whole source-receiver path and it's difficult to isolate the source-side anisotropy, that can be attempted knowing the receiver-side anisotropy and removing it from the seismograms (RUSSO AND SILVER, 1994). A latter possibility is to use ScS, S-wave refracted to the core-mantle boundary that are generated for deep source earthquakes.

There are several advantages of using the SKS: 1) we can analyze the anisotropy beneath the recording station; 2) the phase coming out the fluid core is radially polarised (the P-wave is polarised in the propagation's direction); 3) incidence is nearly vertical (in the 10°cone angle); 4) SKS is an isolated and well recognizable for events occurred at epicentral distance between 85°to 120°.

The last consideration is about the elastic tensors of the medium crossing. In the case of an isotropic medium the elastic constants are simply the Lame's parameters, i.e the bulk modulus (λ) and the shear modulus (μ). The elastic properties of an anisotropic medium can be represented in two main symmetry system, the hexagonal and the orthorhombic one. The orthorhombic symmetry system has three perpendicular axes of symmetry with nine independent elastic constants and describes the general case of anisotropy, considering also the dipping one. The hexagonal symmetry system has 5 independent constants and can be considered the similar case of cylindrical system around a single axis (SAVAGE, 1999). In this case the properties vary in only one direction. When this direction is vertical, we are in the case of radial anisotropy. In the general case the hexagonal symmetry can be consider a special case of the orthorhombic system where two axes have identical speeds.

3.3 METHOD AND DATA

To recover splitting parameters we used a method described in ŠILENÝ AND PLOMEROVÁ (1996). This is a modifications of the most famous SILVER AND CHAN (1991) one but, unlike it, the splitting parameters are determined considering the plane perpendicular to the ray of the shear phase and not only the horizontal plane as in the case of SILVER AND CHAN. In this manner the information from vertical motion are included.

Considering the anisotropy constrained on a single layer with fast axes oriented in the horizontal plane, the splitting parameters are obtained minimizing energy of transverse component after seismogram rotation into a ray-based LQT coordinate system (where L is the ray axis, T the transverse component and Q is orthogonal and coplanar to T). To verify the stability of measurements to noise, values of fast direction and delay are tested using a bootstrapping procedure (SANDVOL AND HEARN, 1994) in which we require the fast polarization to remain stable to random noise fluctuations.

We used data recorded at several seismic stations present in the Northern Apennines (Figure 3.3). The majority of the data were collected by the REtreating-TRench, Extension and Accretion Tectonics

project (*www.geology.yale.edu/RETREAT/index.htm*). The RETREAT project is a multidisciplinary study of the Northern Apennines, funded by the NSF, whose main goal is to develop a self-consistent dynamic model of syn-convergent extension, using the Northern Apennines as naturally laboratory. Its seismological component (MARGHERITI ET AL., 2007) deployed a temporary network from October 2003 and September 2006. It included 50 temporary and permanent sites (Figure 3.3). 10 sets of GAIA instruments were lent by the Geophysical Institute of Prague (squares in Figure 3.3) and recorded for nearly three years from October 2003 to September 2006. Each GAIA station consisted of an STS-2 sensor and a VISTEC digitizer. 25 stations (circles in Figure 3.3) were lent by the PASSCAL program (*www.passcal.nmt.edu*) of the Incorporated Research Institutions in Seismology (IRIS) and recorded for about 2 years, between October 2004 and August 2006. These stations were all equipped with a Reftek130 digitizer; 10 sites had a STS-2 and 15 a CMG-40T motion sensor. These 35 instrument sets were used to cover 39 sites. Many PASSCAL stations were aligned along a transect cutting the Northern Apennines in a NE-SW direction, from the Po-Plain to the Tyrrhenian Sea, named the northern transect (Figure 3.3). Other stations were installed NW and SE of the transect as a cloud. After one year of recordings, in 2005, four stations belonging to the northern transect were moved to another less dense transect southward, from station ELBR, located on Elba island, to station PESR, along the Adriatic coast (southern transect in Figure 3.3). Moreover, to make the RETREAT network denser, data recorded by temporary stations are integrated with those of INGV permanent network and one station, VLC, of the MedNet network. All data recorded on RETREAT sites are archived at the Data Management Center of IRIS (*www.iris.edu*).

We selected all available recordings for 27 teleseismic earthquakes between October 2003 and January 2006, with $M \geq 6.2$ and with an epicentral distance between 85°and 120°(Table 2 in SALIMBENI ET AL., 2008; Figure 3.4). These events give us a good azimuthal coverage, at least for sites recording for longer time intervals; however, events that could be analyzed with back-azimuths from the north and south-west directions, are few. To better isolate the SKS phase in analyzed time windows, most of data were bandpassed with a Butterworth filter between 2 to 100 s.

3.4 MEASUREMENTS AND ANISOTROPIC DOMAINS

We obtained 289 new measurements by SKS splitting analysis that are reported in Table 3 of SALIMBENI ET AL. (2008) and mapped in Figure 3.5 and 3.6. In both maps each symbol is related to a single event-station couple. On the basis of our knowledge of heterogeneities distribution at depth from tomographic studies (LUCENTE ET AL., 1999; PIROMALLO AND MORELLI, 2003), we choose to map the measurements at a piercing point of 150 km of depth. This choice gives a better distinction between measurements

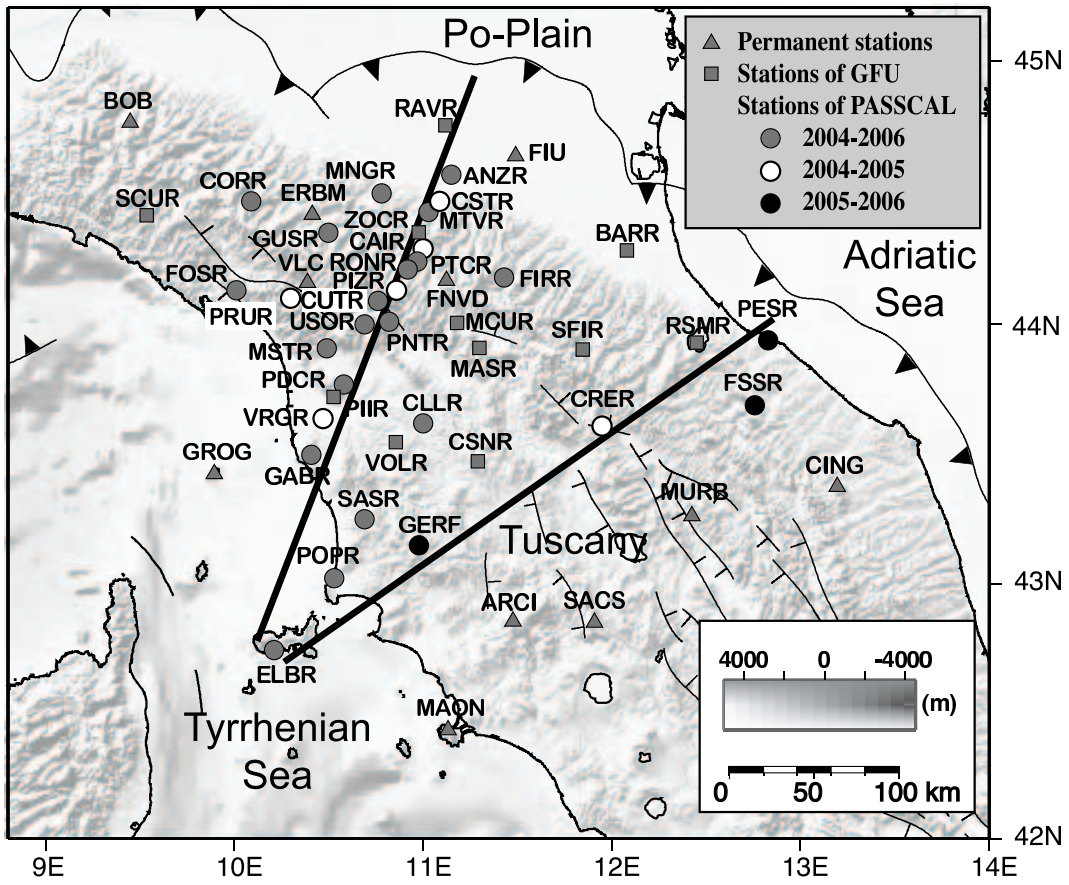

Figure 3.3: Map of the seismic network used in this work. Temporary stations of the RETREAT project are mapped with circles for PASSCAL instruments (with different colors corresponding to different recording time) and with squares for GFU instruments. The triangles represent the permanent stations of the MedNet and INGV networks. The two black lines sketch the northern and southern transects.

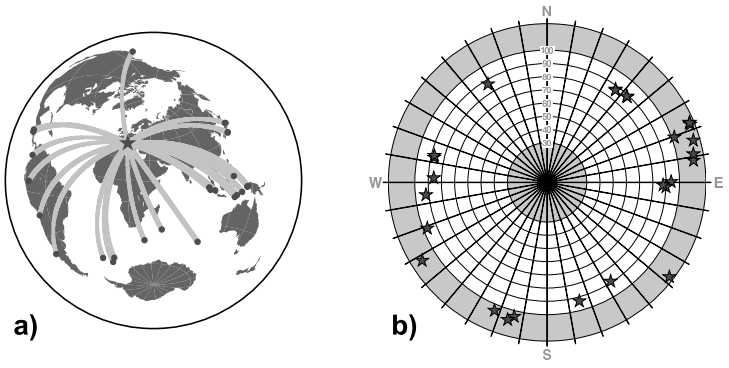

Figure 3.4: *a*) Map of teleseismic earthquakes (dots) used for seismic anisotropy analysis. The RETREAT area is the star. Grey lines are event-station great circle paths. *b*) Azimuthal coverage pattern of analyzed teleseismic earthquakes (black stars). Along the radius is reported the event-station distance (degrees).

done at the same station and makes azimuthal differences more readable. We use also different colors for NE back-azimuth events (-45°to 135°) and SW back-azimuth events (135°to -45°) to further clarify azimuthal variations. This NE-SW distinction is chosen as a boundary to follow the morphological shape of the region where the NW-SE striking direction of the Apennines dominates.

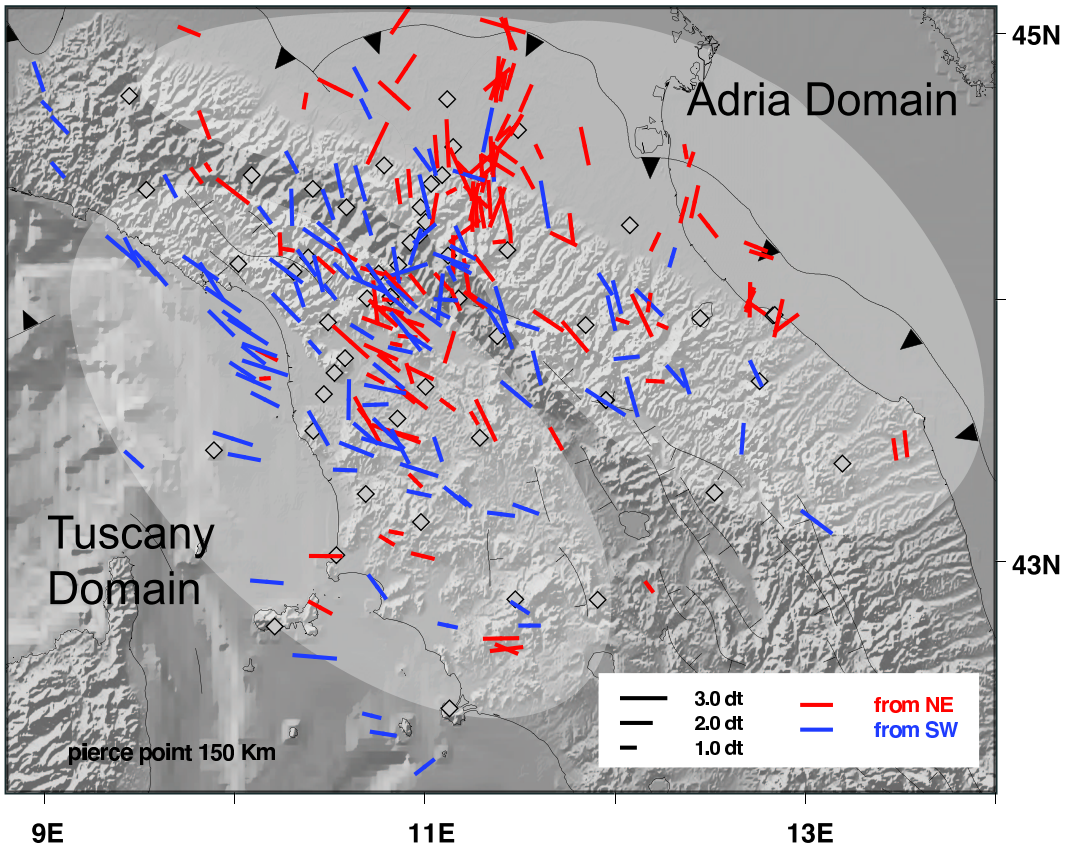

Figure 3.5: a) Map of the splitting measurements reported in Table 3 of SALIMBENI ET AL. (2008). Red color is used for NE back-azimuth events (from -45°to 135°) while blue is for SW events (from 135°to -45°). Single measurements are represented with a line oriented with fast polarization azimuth and scaled with the delay time, mapped at the piercing point of 150 km of depth to give a better distinction between measurements done at the same station and to make azimuthal differences more readable. Shaded zones are Tuscany and Adria domains.

Several null birefringence measurements were obtained (Figure 3.6). We considered a measurement null when there is no energy in the transverse component. The presence of nulls can be interpreted as an absence of anisotropy, but all other measurements assure the presence of anisotropy at depth. Theoretically, a null measurement (i.e., absence of birefringence in the waveform) may reflect either lack of anisotropy, or else propagation of the wave along or normal to anisotropic symmetry axis. Consequently, what is more probable is that the ray paths of studied events are parallel or perpendicular to the anisotropy symmetry axis. For this reason we have mapped null measurements as two crossing-lines

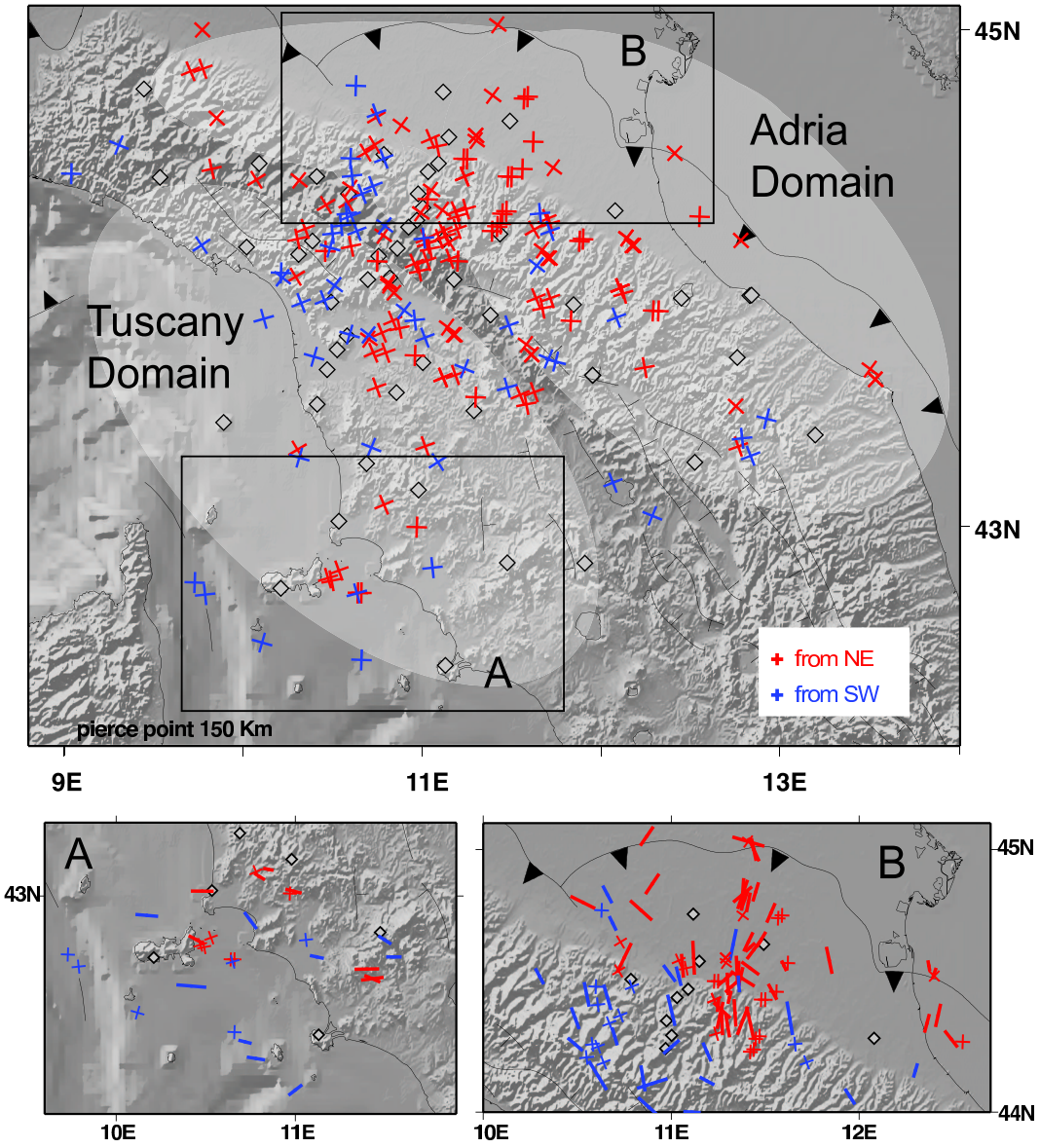

Figure 3.6: Map of the null measurements reported in Table 3 of SALIMBENI ET AL. (2008). Single null measurements are mapped with a cross oriented to the back-azimuth of events. Diamonds represent seismic stations. Inset A and B contain splitting and null measurements for stations inside the two black boxes in the main map.

oriented parallel and perpendicular to back-azimuth. These crossing lines (Figure 3.6) frequently align with single SKS splitting measurements nearby (Inset A and B in Figure 3.6), suggesting often a consistency between them. Figures 3.5 and 3.6 show that, moving from the south-west to the north-east across the Apennines, the orientation of the fast shear-wave polarization direction changes from a dominant NW-SE (orogen-parallel) trend to a NNE-SSW (orogen-normal) main direction. Using the Apennines crest as a boundary we can describe our data starting from the south-western part, i.e., the Tuscany side, where the NW-SE directions are homogeneously distributed from the orogen toward the Tyrrhenian Sea, while a rotation to an E-W direction occurs toward Elba island and also south of it. These directions are corroborated by null measurements (Inset A in Figure 3.6). Delay times have values ranging from 0.6 to 3.3 s, with a 1.8 s on average. Fast velocity directions and delay times do not show a clear dependence on back-azimuths (Figure 3.7a).

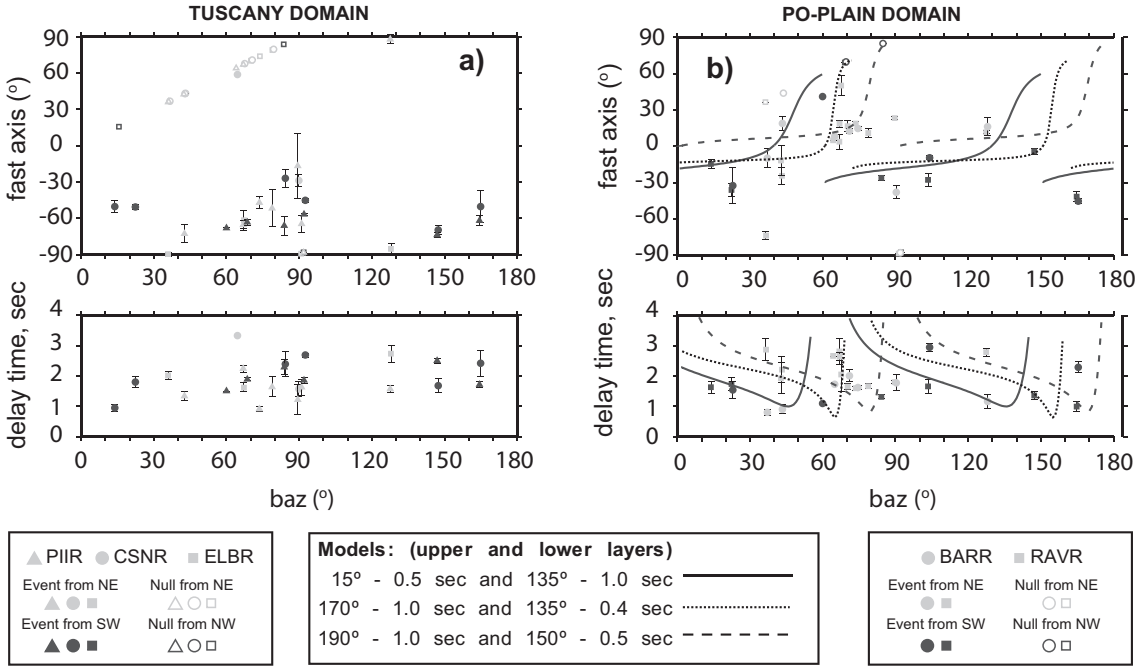

Figure 3.7: Back-azimuth Vs Splitting parameters pattern. Black symbols are used for SW back-azimuth events, gray for NE ones. Null measurements are plotted with empty symbols and with back-azimuth as fast axis. No null measurements are plotted in delay time Vs back-azimuth map. *a)* measurements for PIIR, CSNR and ELBR, that are Tuscany stations, *b)* measurements for stations RAVR and BARR, located in the Po Plain. In the plot on the right the expected behavior of fast polarization azimuths and delay times are reported for three different models of double layer anisotropy determined for the anisotropy parameters value reported in the label.

In the eastern and north-eastern area, that we call the Adria region, the pattern of fast axes is less uniform. A NNE-SSW direction prevails, but NW-SE and N-S fast polarization directions are also detected. Several null measurements support these trends (Inset B in Figure 3.6). Moreover, a dependency on the back-azimuths, already detected for the stations belonging to the northern transect (SALIMBENI ET AL., 2007), exists for all sites on the Adria side: blue symbols in Figure 3.5 strike more frequently in a NW-SE direction and red symbols show mainly N-S and NNE-SSW directions. This behavior would mean that easterly ray paths sample mainly a N-S to NNE-SSW anisotropy, while westerly arrivals cross a medium characterized by NW-SE seismic anisotropy. In the Adria side delay times are $0.8 < dt < 3.2$ s (1.8 s on average), without any noticeable trend. It's important to note that the same average delay time (1.8 s) is found in both sectors, as to indicate that the cumulative thickness of the anisotropic structures beneath the Tuscany and Adria domains is the same.

These two domains are separated by a narrow transition zone (SALIMBENI ET AL., 2007). Analyzing only the 145 SKS birefringence measurements obtained for the northern transect only (Figure 3.8) we can limit the boundary of the transition. In Figure 3.8, values of fast axis are displayed along the array. Nearly 90°rotation in observed fast polarization directions takes place over a transitional region between stations USOR and RONR, in correspondence with the divide of the Apennines, located close to station CUTR. In SWestern region (left side of the plot) fast directions range from 90°to 30°(from E-W to NNW-SSE, grey background, Figure 3.8), with most common directions being between 80°and 60°(limited by dashed lines). In transitional region, we find variable values of fast polarization direction (from 60°to 30°), with presence of both dominant NW-SE fast azimuths in Tuscany and of NNE-SSW azimuths in Po Plain. Variation becomes even more pronounced in Po-Plain, where NW-SE fast direction is mostly absent and N-S and NNE-SSW directions dominate as underlined by rose diagram plots.

RAVR and BARR are the two stations for which we have the richest dataset among those located further NE in the Adria domain. The variability of their anisotropy directions with back-azimuth shows a pattern close to $\phi/2$ periodicity (Figure 3.7b). This suggests that the presence of a double-layer anisotropy beneath Po-Plain should be taken into account. In Figure 3.7 is represented, together with measurements, the expected behavior of fast axis directions and delay times (computed using analytical equations by SILVER AND SAVAGE, 1994 and ÖZALAYBEY AND SAVAGE, 1994) for three different models of double layer anisotropy. Every model assumes horizontal symmetry axes, a cumulative thickness of about 200 km and 5% of anisotropy (MAINPRICE AND SILVER, 1993). Among possible models we chose to plot only three patterns which are more similar to our measurements distribution. In Figure 3.7b, solid line is for an upper and lower layer with respectively fast axis directions and delay times of 15°and 0.5 s., 135°and 1.0 s.; dashed line is for an upper and lower layer with respectively fast axis directions and delay times of 190°and 1.0 s., 150°and 0.5 s.; dotted line is for an upper and lower layer with

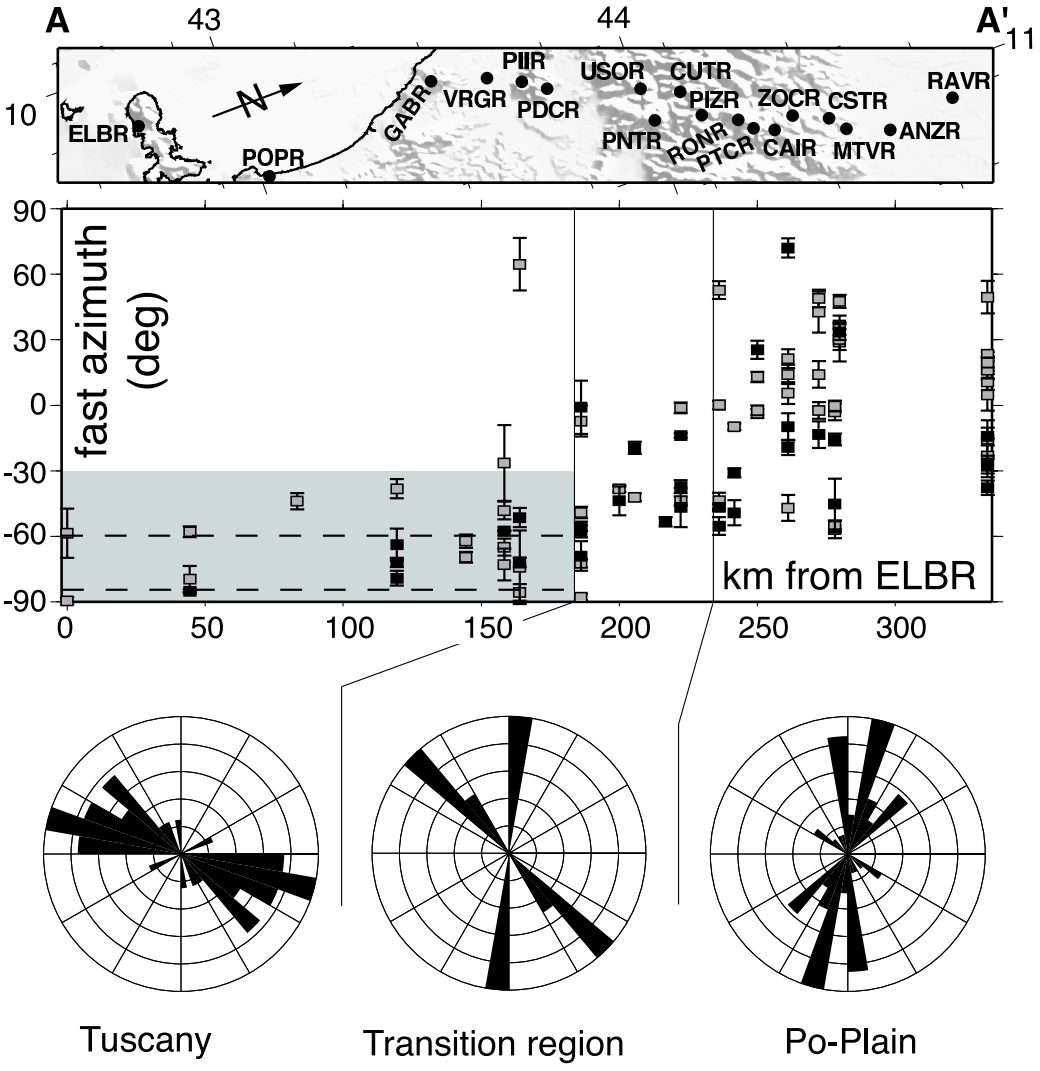

Figure 3.8: Map and plots along the transect (A-A'). Location of stations is in the upper map. Second plot: fast axis directions along the transect. Black and grey symbols are respectively for west and east back-azimuth events. The grey background and the horizontal dashed lines underline the prevalent ranges found for the Tuscany domain. The plot is separated in three part by vertical lines: on the left, data for the Tuscany stations are plotted, in the centre for the transition zone stations and on the right those for the Po-Plain stations. Lower plots: rose frequency diagrams for the three regions.

respectively fast axis directions and delay times of 170°and 1.0 s., 135°and 0.4 s. This latter model shows the best similarity with the periodicity in the data. The number of events coming from different back-azimuths is however not sufficient to characterize the structure beneath each single station (not enough measurements at any of the stations), but the cumulative approach used here gives some more light to some hypotheses.

The geographical variations observed for single measurements are confirmed by the orientations of averaged splitting directions computed as $\frac{1}{2}\arctan\frac{\sum\sin 2\phi}{\sum\cos 2\phi}$ for each station (Figure 3.9). Fast-axis directions rotate gradually from E-W to NW-SE in the Tuscany region, then across the Apennines change to N-S and NNE-SSW in the Adria side. The clockwise rotation is gradual in the southern part of the study region, while more abrupt in the northern part, where the network extends toward the Po Plain. The transition between the two domains is abrupt, about 30 km (SALIMBENI ET AL., 2007) when crossing the orogen along the northern transect. This feature is confirmed along the northernmost part of the study region where, even with larger distances between stations, we see sharp variations in the anisotropy directions between sites separated by 50-60 km (e.g., between PRUR and GUSR or FOSR and CORR, Figures 3.3 and 3.9). Moving southward, along the southern transect, the rotation from one domain to the other occurs between stations 80-100 km away (i.e. compare CRER and FSSR). This suggests that the transition in the southern portion of the RETREAT field area, along the southern transect, could be more gradual than in the north, even if this characteristic could be related to the different distance between stations.

Another feature underlined in the station-averaged birefringence is the non homogeneity of the anisotropy of the Adria region compared to the Tuscany side. Comparing, for individual stations, average fast polarization directions (red arrows on rose diagrams of Figure 3.9) with fast direction frequency distributions (rose diagrams in Figure 3.9), we often find a difference between the most frequent direction and the average one. This occurs at sites located in the transition between the two domains (for instance PNTR, GUSR, RONR, FIRR; Figure 3.9) or located toward the Po Plain (e.g., CSTR, MNGR and RAVR). This discrepancy is more evident when the dispersion of rose diagram is greater, adding more constraints on the hypothesis of structure heterogeneity of this region. In the Tuscany sector, the average and most frequent directions are often nearly the same (e.g., from FOSR, to MAON along the Tyrrhenian coast; Figure 3.9), supporting the idea that measurements here reflect a more homogeneous structure at depth. What seems more interesting in the averaged-birefringence pattern is the regular rotation we observe along the eastern part of the study region, from nearly NNE-SSW trend in central Apennines (e.g., stations PESR, RSMR and SFIR, but see also data from the NAP 8 measured by MARGHERITI ET AL., 1996) to a more NE-SW trend in the Po Plain (i.e., ANZR and RAVR). This is a characteristic feature of sites located on the Adria plate region.

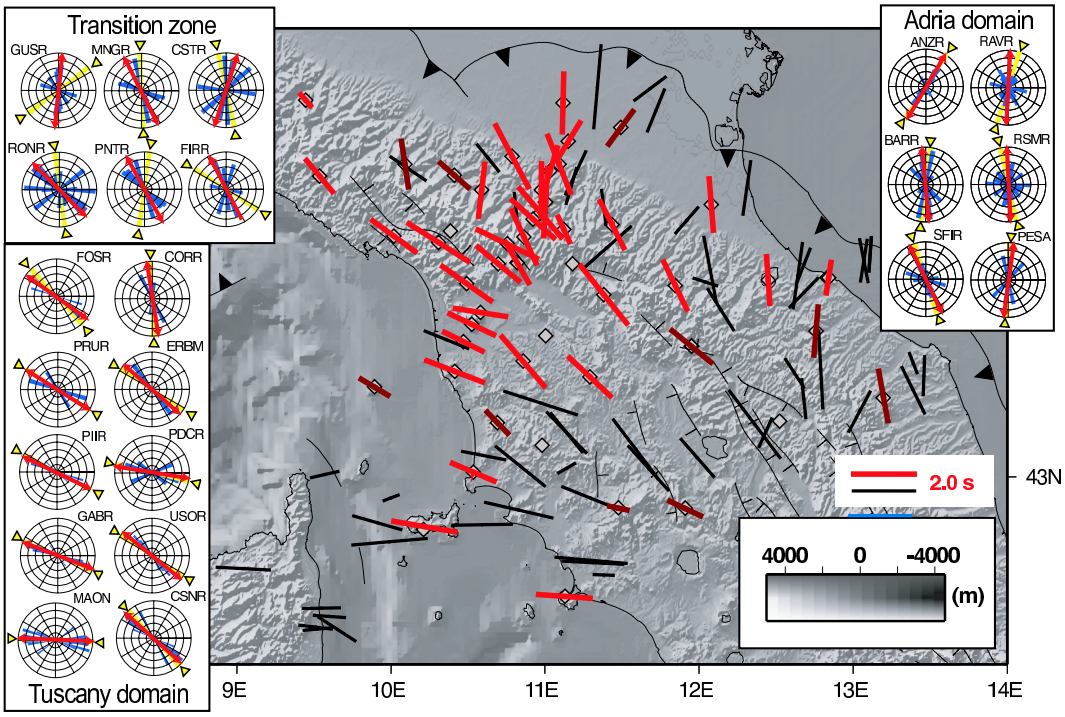

Figure 3.9: Red symbols represent the average fast polarization direction. Dark red is for sites for which the average direction has been computed over less than 4 measurements. Black symbols in the background represent single shear wave splitting measurements from previous papers (PLOMEROVÁ ET AL., 2006; MARGHERITI ET AL., 1996; LUCENTE ET AL., 2006 and reference therein). Boxes include normalized rose diagrams of fast directions for single stations: in blue is the rose diagram, in yellow is the most frequent slice (pointed by two yellow triangles) and the overlapped red arrow is the average direction. Upper left box: rose diagrams for the most representative sites of the transition zone. Lower left box: rose diagrams for the most representative sites of the Tuscany domain. Right box: rose diagrams for the most representative sites of the Adria domain.

3.5 ANISOTROPY VARIATION AT DEPTH

The regional patterns found for the direction of fast polarization have several possible interpretations that we could better discuss having some knowledge of the depth distribution of the anisotropy. As a first approximation, we should take into account that the thickness of the anisotropic medium crossed by our seismic signals should be nearly 200 km, assuming that it is produced by 5% of anisotropy (MAINPRICE AND SILVER, 1993) with horizontal symmetry axis and considering that the average delay time over all the network is 1.8 s. To estimate the depth of seismic anisotropy we study lateral variations of single measurements, having determined them for a dense array. We calculated the Fresnel zones for some of the stations following the approach of PEARCE AND MITTLEMAN (2002), a method which assumes a horizontal fast axis and a lateral variation of the anisotropic properties of the medium. The poor depth resolution intrinsic in the use of SKS and SKKS waves can be improved using singular splitting parameters for a single station analyzing the lateral variation variability of the observed splitting (ALSINA AND SNIEDER, 1995). A single ray-path arriving at a single station is influenced by the elastic properties of the crossed material and can be symbolized as a tube with a diameter of the first Fresnel zone. The size of the Fresnel zone is function of the period and on the travel-time (or length of the ray path). Knowing the size of the first Fresnel zone allows to constrain the anisotropy at depth. In the Northern Apennines we likely have an almost vertical subducting slab (LUCENTE ET AL., 1999), thus it is plausible to assume lateral variations in the anisotropic properties of the mantle; moreover this theory is supported by the existence of geographical domains with different but internally homogeneous anisotropic parameters.

The lateral variation of the anisotropy below a single station, as expressed in variable anisotropic parameters with horizontal symmetry axis, can be resolved by analyzing two teleseismic earthquakes with opposite back-azimuths (Figures 3.10a and 3.10b). The depth defined in this case (Z1) corresponds to the depth above which the ray paths sample the same medium and below which paths are different. If we use observations of only one teleseismic earthquake recorded at two or more nearby stations (Figures 3.10c and 3.10d) we can evaluate the depth (Z2) where the two ray paths start to separate. Differences in birefringence parameters would be due to an anisotropy located at a depth above the point where paths separate.

The Fresnel zones at depth h are calculated following (PEARCE AND MITTLEMAN, 2002):

$$Rf = \frac{1}{2}\sqrt{T\nu h} \tag{3.2}$$

where Rf is the radius of the Fresnel zone expressed in km, T is the dominant period of the wave and ν is the wave velocity. We choose 10 s for the dominant period from waveform observations and the shear-wave velocity of the S phases from IASP91 model (4.476 km/s at 50 km depth, 4.49 km/s at 100

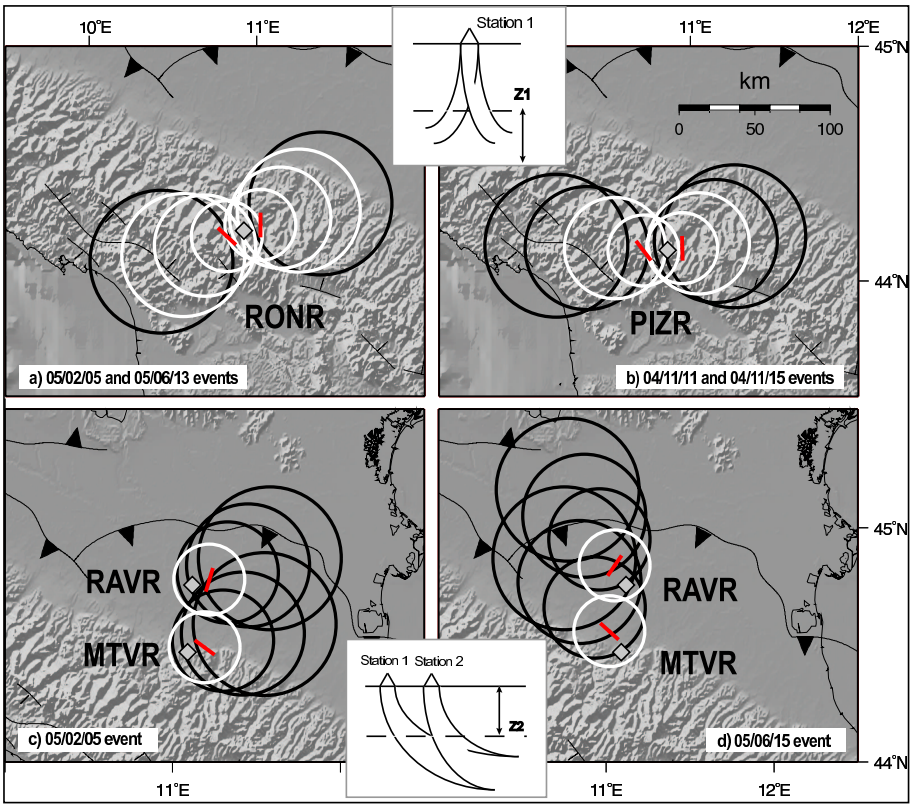

Figure 3.10: Fresnel zone analysis for some stations located along the northern transect (*a* and *b*) and in the Po-Plain sector (*c* and *d*). Different dimensions of circles correspond to Fresnel zones calculated at 50, 100, 150 and 200 km of depth respectively. For each station-event pair also the fast polarization azimuth is mapped at 50 km pierce point. Assuming horizontal symmetry axis, relevant circles to determine values of Z1 (depth below which difference in anisotropy are sampled) and Z2 (depth above which difference in anisotropy are sampled) are in white. Upper central inset: sketch of the determination of Z1, applied in examples *a* and *b*. Lower central inset: sketch of the determination of Z2, applied in examples *c* and *d*.

km depth, 4.45 km/s at 150 km depth and 4.51 km/s at 200 km depth).

We applied this method for some stations located within the transition between Tuscany and Adria domains (Figure 3.10). For station RONR (Figure 3.10a), located close to the Apennines crest, we obtained two different measurements analyzing two events with opposite back-azimuth. The Fresnel zones reveal that this difference may be due to a different anisotropy sampled by the ray-paths below a depth of 150 km, at which rays separate (and circles in Figures 3.10a and 3.10b do not cross anymore). In the case of station PIZR (Figure 3.10b), located close to RONR, we can observe that beneath the crest of the chain the anisotropy has a lateral variation below a depth between 100 and 150 km: in the west (Tuscany domain) the fast polarization is NW-SE and in the east (Adria domain) it is nearly N-S. We consider also the ray-paths for two different events recorded at nearby stations to constrain the lower boundary of the region where anisotropy changes laterally: at the transition between Tuscany domain and Adria domain no resolving examples were found. On the other hand, in the Adria side, at stations RAVR and MTVR measured anisotropic parameters for the same event are different (Figures 3.10c and 3.10d). This difference is due to changing anisotropy sampled above 50 km of depth, where the paths of the two rays separate significantly (and circles of Figures. 3.10c and 3.10d do not cross anymore). This behavior occurs for two events coming from different back-azimuths, reinforcing the idea that another lateral variation occurs in the upper 50 km in the Adria domain between the chain and the Po-Plain.

These considerations about the distribution of the anisotropy at depth can also be compared to mantle velocity structure depicted by seismic tomography. Plotting possible SKS ray-paths over a tomographic section we can define which structures are sampled. The two tomographic sections (Figure 3.11; PIROMALLO AND MORELLI, 2003) cross the Northern Apennines in two different directions. In the green section, the E-W directions measured at station ELBR can be certainly attributed to the mantle wedge that is mainly crossed by the ray-paths (black lines in Figure 3.11). This interpretation can be extended also to measurements done for stations south of 43.5N, from GROG to MAON (Figure 3.3). The NW-SE directions found at station PIIR instead can be related mainly to the slab and mantle immediately below the slab, taking into account that mantle wedge is too thin beneath this station compared to the 200 km thickness needed by birefringence delay times. Beneath station RONR the Fresnel zones analysis demonstrates the presence of a lateral variation between two anisotropy domains (NW-SE and N-S) below 150 km. Following SKS paths beneath this station we can suppose that events from the west sample the anisotropy located in the slab and in the mantle just beneath it (NW-SE) and those from the eastern back-azimuths sample the Adria mantle (N-S to NNE-SSW). We hypothesize that the mantle below Adria just beneath the slab and at some distance from it underwent different deformations. The mantle just beneath the slab was deformed directly by the retreating process (BUTTLES AND OLSON, 1998) showing a fast direction parallel to the strike of the slab while farther in the foreland the dominant N-S fast direc-

tion cannot be ascribed to the same process. For station RAVR , all SKS rays sample the mantle beneath Adria, in spite of their variability. In the red section (Figure 3.11) we observe that some rays reaching the station ELBR from the east sample slab anisotropy; very few measurements (Figures 3.5 and 3.6) show a NW-SE rather than an E-W direction. For station CSNR the SKS splitting data sample the slab and sub-slab mantle deformed by retreat, and show homogeneity of NW-SE fast axes. Station RSMR is above a less perturbed portion of the Adria domain where the only source of anisotropy has roughly N-S fast direction.

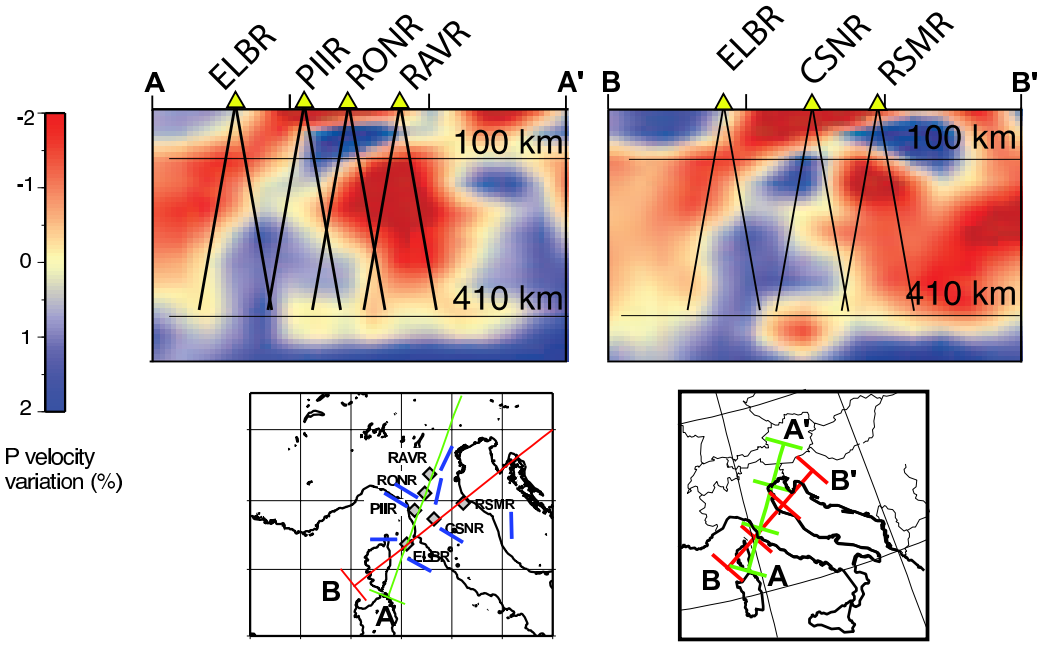

Figure 3.11: Tomographic sections across the Northern Apennines (from PIROMALLO AND MORELLI, 2003) and sketch depiction of regions sampled by SKS ray paths ascending towards stations on the surface. 100 and 410 km depths are drawn by thin lines. Lower left: map of stations reported along the sections, with orientation of fast polarization azimuths at these sites (in blue). Also section lines (red and green) are mapped. Lower right: section lines.

Chapter 4

MODELING COMPLEX ANISOTROPIC STRUCTURES

In last chapter we have shown the splitting parameters measured for each single station installed in the Northern Apennines. Following the distribution of these results we have defined two main anisotropic domains: the Tuscany domain in which measurements are well distributed as E-W and NW-SE, Apenninic directions, without back-azimuthal dependence; the Adria domain in which fast polarization directions are not homogeneous, with NE to NNE-SSW and NW-SE directions, and these measurements have also a back-azimuthal dependence.

The variations in splitting parameters as function of the direction of propagation is referred as due to the presence of heterogeneous anisotropy in the first 250 Km ok depth (SAVAGE, 1999). It could occur in homogeneous medium if the anisotropy symmetry system is complex (i.e. orthorhombic) considering parameters measured for different polarization, back-azimuth or incidence angles. In the case of complex symmetry systems the measurements of splitting are interpreted as apparent (SAVAGE 1999) i.e. generated from earth structures composed by more than one layer or dipping axis symmetry. This consideration could be showed in the distributions of the splitting parameters as a function of back-azimuth of the analyzed events; they show a 90°periodicity in the case of multilayer anisotropy (SILVER AND SAVAGE, 1994; RÜMPKER AND SILVER, 1998; LEVIN ET AL., 1999; SALTZER ET AL., 2000) or a 180°periodicity for dipping axis (PLOMEROVÁ ET AL., 1998; HARTOG AND SCHWARTZ, 2000).

In the case of Tuscany measurements, this periodicity is not observed (Figure 3.7a) so, it is more plausible that beneath the region exists a simple anisotropic structure composed by a single anisotropic layer with fast axis in the horizontal plane. The 90°periodicity is instead present in the data distribution of the Adria region (Figure 3.7b) so the presence of a multilayer structure beneath it can be hypothe-

sized. To verify this idea we used the cross-convolution method of MENKE AND LEVIN (2003) that allows to model a multilayer structure using SKS splitting analysis.

4.1 CROSS-CONVOLUTION METHOD: A TWO LAYERS STRUCTURE

The Cross-convolution method (MENKE AND LEVIN, 2003) is a technique for determining the structure of anisotropy of the earth using observations of shear waves splitting (such as SKS). After the waveform-matching procedure, the method tests predictions from models against observed waveforms. It uses this predictions as an input of a systematic model-fitting grid search to determine the best-fitting anisotropic model. The methodology is not based on apparent splitting parameters concept as single event-station shear wave splitting analysis (i.e they are not interpreted in the context of directional dependence) and does not contain prior assumptions concerning the process affecting the waveforms. Indeed, events from all back-azimuths are used together.

The method looks for the conditions at which seismic waveforms are consistent with a one-layer or multilayer anisotropic earth structure beneath a station having N splitting teleseismic signals with different incident angles and back-azimuths. If the radial-horizontal and tangential-horizontal seismograms are denoted by $V_i^{obs}(t)$ and $H_i^{obs}(t)$, both observed components are defined as

$$\begin{aligned} V_i^{obs}(t) &= s_i(t)^{true} * v_i(t)^{true} \\ H_i^{obs}(t) &= s_i(t)^{true} * h_i(t)^{true} \end{aligned} \tag{4.1}$$

where $s_i(t)^{true}$ is the source wavelet characterizing the waveform of the phase before it interacts with the anisotropic structure. It describes both the effects of the earthquakes source than subsequence structures modification far from the stations. $v_i(t)^{true}$ and $h_i(t)^{true}$ are radial and tangential impulse response functions and the term *true* denote impulse response functions in absence of noise.

We suppose to have a model *m* for the near-receiver earth structure as a vector containing real splitting parameters (corresponding to our unknown quantities) and we assume to know the way to define the predicted impulse response functions $v_i(m,t)^{pre}$ and $h_i(m,t)^{pre}$. The predicted seismograms are

$$\begin{aligned} V_i(t)^{pre} &= s_i(t)^{true} * v_i(m,t)^{pre} \\ H_i(t)^{pre} &= s_i(t)^{true} * h_i(m,t)^{pre} \end{aligned} \tag{4.2}$$

To find which model best fits the predicted and the observed seismograms we can remove the source

wavelet component and convolve the first term in 4.1 with $h_i(m,t)^{pre}$ and the second with $v_i(m,t)^{pre}$ obtaining

$$h_i(m,t)^{pre} * V_i^{obs}(t) = s_i(t)^{true} * v_i(t)^{true} * h_i(m,t)^{pre} \tag{4.3}$$
$$v_i(m,t)^{pre} * H_i^{obs}(t) = s_i(t)^{true} * h_i(t)^{true} * v_i(m,t)^{pre}$$

A good model have to satisfy $v_i(m,t)^{pre} \approx v_i(t)^{true}$ and $h_i(m,t)^{pre} \approx h_i(t)^{true}$, therefore m have to satisfy

$$h_i(m,t)^{pre} * V_i^{obs}(t) \approx v_i(m,t)^{pre} * H_i^{obs}(t) \tag{4.4}$$

Its least-square minimum is the best model fitting observed and synthetics seismograms

$$E(m) = \frac{1}{N}\sum_{i=1}^{N} \left\| h_i^{pre}(m,t) * V_i^{obs}(t) - v_i^{pre}(m,t) * H_i^{obs}(t) \right\|^2 \tag{4.5}$$

$E(m)$ is zero for a perfect fitting, while it is close to 1 in the case of a poor fit.

To apply the formulation above to a model composed by one anisotropic layer defined in a reference frame with radial-horizontal direction pointing toward the source and the tangential-horizontal direction to be 90°counterclockwise from the radial-horizontal direction, these relations need to be satisfied:

$$v_i(m,t)^{pre} = a_1\delta(t) + a_2\delta(t-\tau) \tag{4.6}$$
$$h_i(m,t)^{pre} = b_1\delta(t) + b_2\delta(t-\tau)$$

where τ is the delay time, θ the fast axes direction, ϕ the back-azimuth of the source and $a_1 = \cos^2(\theta-\phi)$, $a_2 = \sin^2(\theta-\phi)$, $b_1 = -b_2 = \cos(\theta-\phi)\sin(\theta-\phi)$. The one layer model have two unknown parameters, τ and θ. Similarly to this case is the double layers one, with more complex formulations because the parameters to define are four, the anisotropic parameters for the upper and lower layers.

In all cases, delay and fast direction parametrization of the layered models assumes horizontal axes of anisotropic symmetry, and the description of models does not say anything about the thickness of layers involved, the strength of anisotropy is not determined, but only the effect on a vertically-propagating S wave.

4.1.1 DATASET USED

We selected all teleseismic events with $M \geq 6.0$ occurred from October 2003 to September 2006 recorded by the seismic station installed in the Northern Apennines (Figure 3.3). To guarantee the presence of

the SKS (and SKKS) phases in our data, all the events selected have an epicentral distances ranging from 85°to 120°. All recordings are provided by the IRIS Data Management Center (*www.iris.edu*).

Our dataset have been recorded by different kind of instruments belonging to different networks present in the area, so it has been necessary to filter differently the data. The typical used bandpass filter was between 0.01 Hz to 0.2 Hz but in some cases, as for the most noisy Adriatic stations, the range is restricted to 0.01 Hz to 0.1 Hz. For result homogeneity, all the data are also sampled at 20 sps and cut in a window of 80 s.

The first step is to calculate for each events the shear wave splitting parameters at a given station. These observations are calculated using different methods. One finds splitting azimuth and delay time maximizing the cross-correlation between rotated seismograms. The second estimates simple one-layer anisotropy parameters from a single radially-polarized phase using cross-convolution method (MENKE AND LEVIN, 2003). Comparing the results, we choose that events that provide a difference between real back-azimuth and re-calculated polarization lower than 15°. After this selection, all of events with misfit lower than 0.4 are used as input into the group inversion.

The inversion provides two results. One is obtained for a structures composed by one anisotropic layer with horizontal anisotropy; the second one is for two anisotropic layers. The model that is considered the more convincing is the one that gives a real improvement in the misfit for the group inversion. Examples of analyses are shown in Figures 4.1 and 4.2. In both figures are shown the results of group inversions for one-layer (left plot) and two-layer structures (right plot). For a one-layer structure is shown the misfit value surface plot and the best-fitting model (the star) corresponding the values of anisotropic parameters which minimize the misfit between recorded SKS and synthetic waveforms. The error surface plot for double-layer structures reports in color the area where the double-layers solution have a lower misfit than the one-layer one while in white where the error is greater. Also in this case the star represents the minimum value. When the surface that represents the difference between errors in one and two layer results is wide, we consider the second one the best-fitting model (for example MAON, Figure 4.1) otherwise we considering the one layer the best-fitting one (i.e., CSNR, Figure 4.2). To choose the best fitting two layers model, the final solution is selected over the range of possible solutions excluding those with delay times ≥ 3.0 s. and differences between the fast axes orientations of the two layers ranging around 90°(avoiding near-normal fast polarization values in which the effect of one layer cancels the effect of the other).

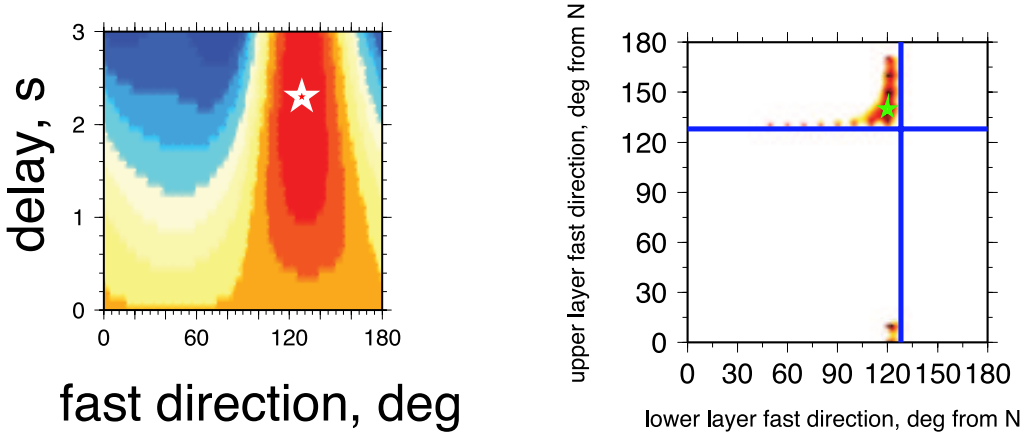

Figure 4.1: Results of the group inversion for CSNR station. Plot on left shown values of the data fit measure for one-layer solution. Plot on the right instead shown error surface for the two-layer cross-convolution method. All regions where the error is greater than the best-fitting one-layer solution are in white. In both plots, star indicate the global minimum. In this case, one-layer model is the best solution.

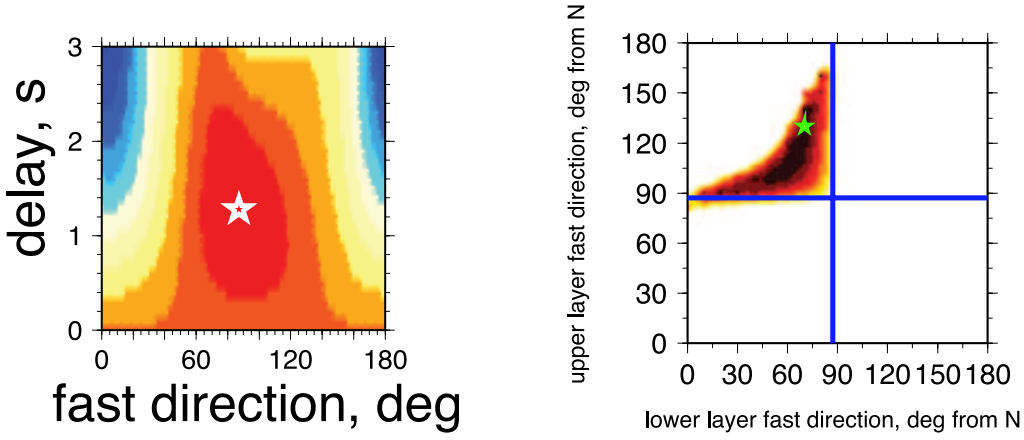

Figure 4.2: Results of the group inversion for MAON station. Plot on left shown values of the data fit measure for one-layer solution. Plot on the right instead shown error surface for the two-layer cross-convolution method. All regions where the error is greater than the best-fitting one-layer solution are in white. In both plots, star indicate the global minimum. In this case, two-layer model is the best solution.

4.1.2 RESULTS FOR A TWO ANISOTROPIC LAYERS MODEL

The results obtained for each station for which this analysis has been done in Northern Apennines are mapped in Figure 4.3. Stations for which the best-fitting solution is the one layer model are mapped using a a green stick, representing the anisotropic parameters obtained from the inversion. Stations for which the two layers model is the best are reported on map using a rose diagram composed of red and black sticks. In red are drawn sticks representing the splitting parameters of the lower layer while in black are the values for the upper layer. Given the broad range of possible solutions, all in a small interval of variance reduction we plot only the 10 solutions with lower misfit, both for the single than for double layer solutions.

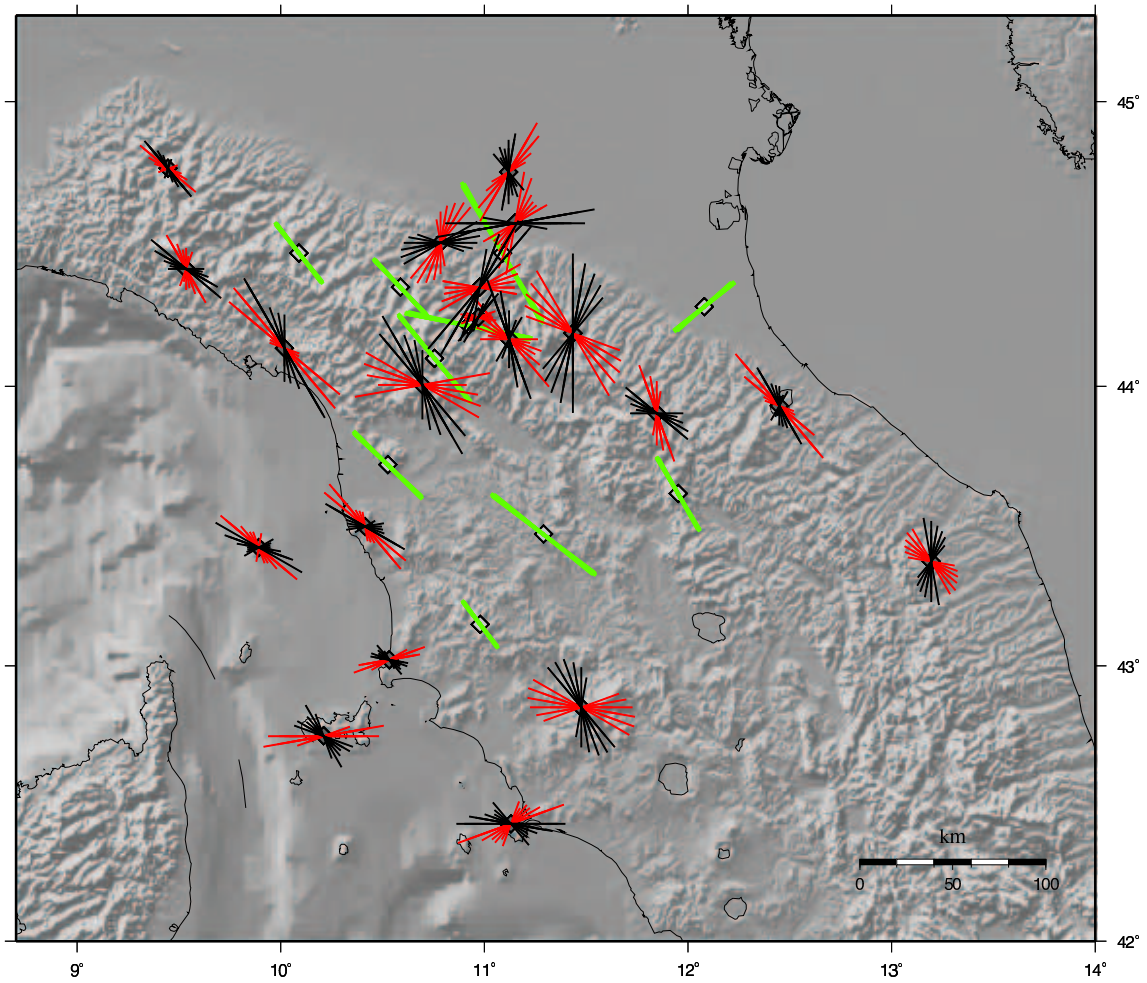

Figure 4.3: Shear wave splitting results of the cross-convolution inversion for Northern Apennines. In green are represented splitting parameters for one layer model, in red the splitting parameters for the lower and in black for the upper two layer's models.

Having a group of SKS observations for each station, the anisotropic parameters assuming the best

single anisotropic layer model and the best double anisotropic layers structure are found in a grid search. The best set of anisotropic parameters values is determined on the basis of the variance changes among all the solutions. In the interpretation of results some particular cases should be taken into account. For instance in the case of two layers of equal thickness and crossed anisotropy the results are consistent with both one and two layers structure. In fact, one layer can be made arbitrarily thicker if one chooses the polarization of the other layer to cancel out the increase. Another particular case which needs much care in the interpretation is when the data are noisy. In this case the double layer structure results can fit the noise, but providing a solution that doesn't improve the fit in a significant manner respect the one layer one. Moreover, the result show two dissimilar delay time and fast axes that are nearly 90°apart. This last is named nearly one-layer two-layer solution and it doesn't arise if the data are really fitting a two-layer earth structure and as long as the fast directions are not perpendicularly crossed.

The modeling of deep earth structures showed in Figure 4.3 for the Tuscany domain seems to be homogeneous and in agreement with single shear wave splitting measurements (Figures 3.5 and 3.6). One anisotropic layer solution is the best for most of the stations located in the inner part of the chain with split oriented in NW-SE direction (Apenninic direction). Along the coast and in the Tyrrhenian Sea the double layers solutions is the best one. The stations located south of 43°(MAON, ELBR, ARCI and POPR) have more differences between fast axes directions of the upper and lower layers. In the upper layers, the fast directions determined are mainly NW-SE and become E-W moving to south, exactly as the fast axes distribution showed by single shear wave measurements (Figure 3.5). The fast axes directions attributed to lower layers are nearly E-W and WSW-ENE. For the stations north of 43°these differences become less visible. The fast axes directions for the upper and the lower layers are really similar, mainly NW-SE trending. Given this parallelism we could interpret the earth structures beneath these stations however as a one layer structure with the fast axes in an Apenninic directions, confirming the single shear wave splitting measurements results.

In the Adria domain and in the transition zone the results are far to be clear. Looking into zoomed areas (Figure 4.4) an homogeneous distribution of the fast axes for both one than two anisotropic layer could be visible only in the inner part of the chain, from GABR to CUTR.

Moving along the transect, from RONR to RAVR, this kind of agreement disappeared and the measurements are scattered in all directions. Locally some homogeneity can be observed; similar one layer directions of RONR and lower layers of PTCR and ZOCR, even if delays time have a big difference; parallel directions in lower layers but disagreement between in upper ones for FNVD and FIRR; MNGR, ANZR and RAVR have NNE-SSW directions for lower layers while disagreement occurred for upper layers directions (MNGR and ANZR have a E-W, ENE-WSW direction while RAVR have N-S to NNW-SSE). The one layer structure found for MTVR stations disagree with other close station. For this station, the

mismatch, associated with the high delay time (close to 3.0 sec) is probably due to scarce quality of data (only 13 events used and not all of good quality).

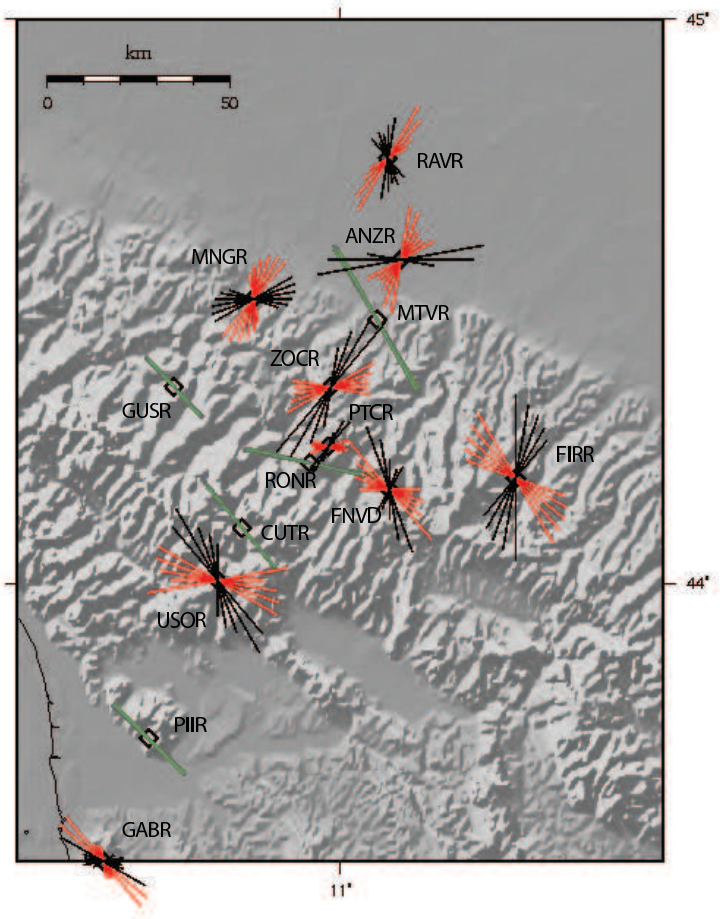

Figure 4.4: Shear wave splitting results of the cross-convolution inversion for Adria and transition zones. In green are represented splitting parameters for one layer model, in red the splitting parameters for the lower and in dark for the upper two layer's models.

Chapter 5

DISCUSSION AND CONCLUSIONS: A CASE OF OBLIQUE TRENCH RETREAT

In this thesis we studied the deformation pattern in the crust and at depth (using seismological data) of the Northern Apennines with the aim to sketch the geodynamic model that produced the Northern Apennines as it is today. As concern the crust deformation, the single moment tensors and the summations we computed show as in the inner part and along the crest of the chain, the deformation is extensional, with T-axes mainly oriented in NW-SE direction. This occurs in the first 15 Km of crust while deeper, between 15 to 40 Km, extensional deformation disappears (i.e. in Tuscany) and only beneath the Apuane and Central Apennines remains. In the outer part of the belt instead the deformation is compressional with NE-SW to N-S maximum compressional direction (given by P-axes) at all depths; below 15 Km however it migrates beneath the crest of the chain. Strike-slip deformation occurs mainly in the western part of the Northern Apennines, in the Alps-Apennines transition. In Tuscany, as the extensional deformation, also strike-slip deformation is mainly in the shallower part of the crust. Extensional and compressive deformations are separated by a sharp transition in correspondence of the Apennines divide (PONDRELLI ET AL., 2006, Figure 2.5). Observing the pattern shown by the seismic deformation obtained by moment tensors summation, together with the distribution of the different moment tensors in the region and at depth, we can say that two deformation domains exist. In Tuscany the extension prevails and in the Adria region the deformation is mainly compressional. Strike-slip deformation is substantially present in the northern part of the region with most frequent distribution in the Alps-Apennines transition zone and in the Apennines-Po-Plain zones.

These results are in agreement with previous works about moment tensors (PONDRELLI ET AL., 2002; 2004a; 2007; VANNUCCI ET AL., 2004) about GPS measurements (SERPELLONI ET AL., 2005), seismicity

(CHIARABBA ET AL., 2005; FREPOLI AND AMATO, 1997) and active stress studies (MONTONE ET AL., 1999, 2004).

Many authors (DEWEY ET AL., 1989, FACCENNA ET AL. 2004, SCROCCA ET AL. 2007 or PICCOTTI AND PAZZAGLIA, 2008) describe this deformation pattern in the crust as due to the slab-retreat action occurred during E-ward migration of the Apenninic front. In this geodynamical model, the closely juxtaposed contraction and extension are the result of the accretion of crustal material from the subducting plate and of the stretching of the upper plate by slab-retreat, respectively. This process is coupled by mantle flow due to the retrograde motion of the slab respect to the surrounding mantle.

The analysis of seismic anisotropy gives us information about this mantle deformation. With this thesis we have increased enormously the number of splitting measurements in the Northern Apennines region. Previous studies had only sparse measurements (PLOMEROVÁ ET AL., 2006) that, added with our data, allow to draw two domains with different anisotropic pattern: the Tuscany and Adria regions. The crest of the Apennines marks the boundary between them, along the whole RETREAT deployment (SALIMBENI ET AL., 2007). In the Tuscany domain fast axis are mainly oriented in NW-SE direction and rotate to E-W moving to the Tyrrhenian Sea. In the Adria domain instead the measurements are sparse, with most frequent measurements in NNE-SSW direction, but also N-S or NW-SE. The average distribution of the fast axis directions show a general rotation that from E-W in Tyrrheanian Sea changes to NW-SE beneath the crest of the belt and becomes N-S in the Adriatic region. This rotation isn't so clear in the northern part of the study region but it is evident in the southern part where our results are similar to those obtained in previous studies (MARGHERITI ET AL., 1996; BARRUOL ET AL., 2004) in which the typical slab roll-back anisotropy directions were found.

The pattern of fast polarization directions characteristic of a retreating-trench system, parallel to the trench beneath the mountains and perpendicular to it in the back-arc basin (Figure 5.1a, b), is not present in the north of our study region (Figure 5.1c). To explain this observation, we related the anisotropy pattern to the history of the trench retreat (FACCENNA ET AL., 2004). When the trench was still striking N-S, west of Corsica, we can suppose that the slab was retreating eastward, normal to the Corsica-Sardinia axis (Figure 5.1a). Subsequently, the process of slab roll-back and trench retreat has proceeded but the prevalent retreat direction was E-W, normal to the southern edge of Northern Apennines (SNA in Figure 5.1b and c). At the same time, the northernmost part of subduction (NNA in Figure 5.1c) moved in an oblique direction relative to trench strike, pulled by nearly eastward roll-back to the south (NNA in Figure 5.1c). The most recent history of the Northern Apennines would then include subduction with a differential roll-back. A maximum eastward retreat would have acted in the southern edge of Northern Apennines, perpendicular to the trench in the center of the arc; at the northernmost corner an ancillary retreat, oblique to the trench, would consequently have occured. The

back-arc region of the corner edge was too small to produce an orogen-normal deformation. This mechanism explains our observations better than a radial homogeneous retreat along the Northern Apennines arc which would have produced the pattern in Figure 5.1b.

We can observe also that the northernmost part of the Northern Apennines is less developed respect to its southern part; it is about 300 km wide from the Tyrrhenian Sea to the Po Plain, compared to the situation at south, where the retreat produced a 600 Km wide system. Also at depth the sub-slab mantle deformed by roll-back seems to be narrower beneath the northern most part of the Apennines, where the slab is also more vertical compared to what tomography images show beneath south-Northern Apennines (Figure 3.11). The oblique retreat would moreover be in agreement with the distribution of the different tectonic regimes detected by shallow deformation study. Extension and compression seismic deformation are justapposed where the retreat developed regularly, while strike-slip deformation prevails where the trench and the retreat direction were not perpendicular.

The less advanced evolution of the Northern Apennines retreat may be due to several reasons among which we firstly would list its position near the northern hinge of the chain. Also it is possible that the Adria plate, either continental or transitional in lithology, resisted subduction, becoming an obstacle for the retreat process. The composition and thickness of the Adria microplate is not known to vary greatly along the Northern Apennines, however, so kinematic factors may be more important. The Alps lie close to the north, and may have behaved as a barrier for the retreat to proceed.

Another possible interpretation of our measurements could be linked with the presence of a discontinuity in subducting slab. A tear in the slab beneath the northernmost corner of the Apennines orogen, and mantle flow through it, would be a possible consequence of the shear occurring during the oblique retreat in the northernmost part of the Apennines. Such mantle flow could explain the NNE-SSW directions detected for the Po-Plain sites. However, the absence of any disruption of the NW-SE direction found for all measurements on the Tuscany side does not support a fully developed slab-window flow. This is confirmed also by earth structures modeling work. If the tear exists, therefore, it is in an early stage and no mantle through-flow has occurred.

The modeling of complex anisotropic earth structure confirms only in part this re-constructions. In Tuscany, we can hypothesize that data recorded at stations located north of 43°sampled only the mantle wedge in the case of one layer structure, with NW-SE anisotropy. The parallelism between fast axes of upper and lower layers can be linked with the sampling of the mantle wedge and part of the slab. South of 43°, all the stations analyzed have a double layers solutions. The direction of the upper layers are mainly NW-SE interpreted with the fact that the waves sampled the slab and the mantle wedge. The direction of the lower layers instead are in agreement with a mantle flow due to the action of the complete retreat process including the opening of the back arc Tyrrhenian basin (Figure 5.1b).

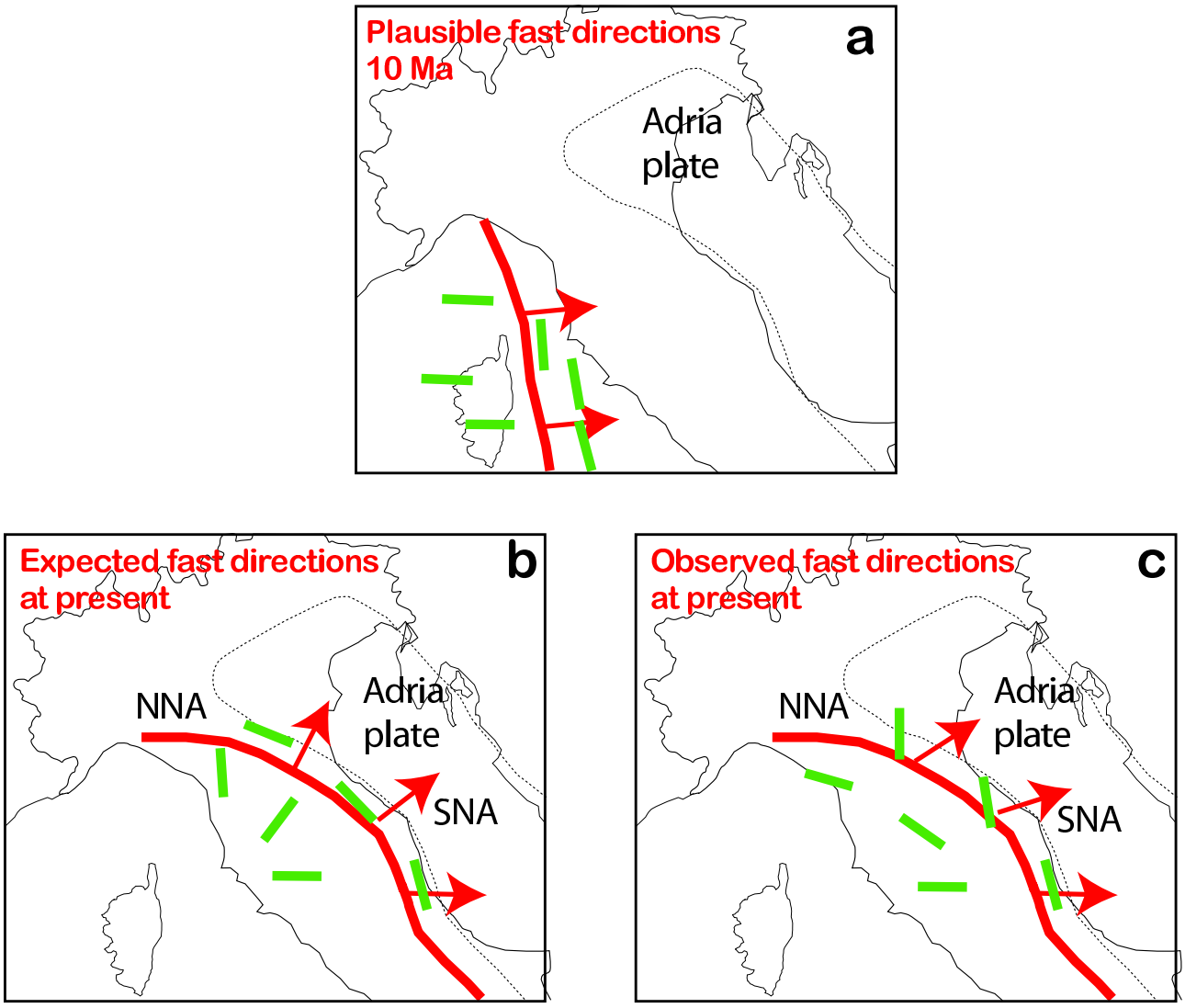

Figure 5.1: Maps of the retreat process history in three possible phases of evolution following the position of the trench (red lines). Green sticks represent anisotropy orientation of fast velocity direction. *a)* possible fast polarization directions during an homogeneous retreat process; *b)* expected fast polarization directions at present if retreat subduction process would have been homogeneous; *c)* fast polarization directions that we find and that is better justified with an oblique trench retreat. NNA: the northernmost part of the Apennines. SNA: southern edge of Northern Apennines. Dotted line shows the Adria plate boundaries.

The Adria domain is characterized by a N-S anisotropic fast polarization in its southern part, in agreement with data from previous studies (MARGHERITI ET AL., 1996; 2003) and by more scattered fast-polarization directions to the north, in the Po River Plain. The double-layer models we obtained, integrated in this deformational pattern, doesn't improve the interpretation of the variability. The directions for upper and lower layers are very sparse and are non-homogeneously distributed between closely stations. The agreement is difficult also comparing stations which match with one layer solution. Given the particular location of the area, the presence of a slab and the vicinity with the Alps a plausible answer is that beneath this area the upper mantle is more complex than a structures with double layers and horizontal anisotropy. In this area additional modeling of anisotropy structures are necessary (i.e. dipping anisotropy).

Bibliography

[1] Alsina D., and R. Snieder, *1995*, Small-scale sublithospheric continental mantle deformation; constrain from SKS splitting observations, Geophys. J. Int., 123, 431-448.

[2] Arvidsson R. and G. Ekström, *1998*, Global CMT analysis of moderate earthquakes Mw $\geq$ 4.5 using intermediate period surface waves, Bull. Seismol. Soc. Am., 88, 1003-1013.

[3] Augliera P., Bethoux N., Deverchere J., C. Eva, *1994*, The Ligurian Sea: new seismotectonic evidence, Boll. Geof. Teor. Appl., XXXVI, 363-380.

[4] Bajc J., Aoudia A., Sarao A., P. Suhadolc, *2001*, The 1998 Bovec-Krn Mountain (Slovenia) earthquake sequence, Geophys. Res. Lett., 28, 1839-1842.

[5] Bally A. W., Burbi L., Cooper C., and R. Ghelardoni, *1986*, Balanced sections and seismic reflection profiles across the central Apennines, Mem. Soc. Geol. It., 35, 257-310.

[6] Barchi M., Minelli G., and G. Pialli, *1998*, The CROP-03 profile. A synthesis of results on deep structures of the northern Apennines, Memorie Societá Geologica Italiana, 52, 383-400.

[7] Baroux E., Béthoux N., and O. Bellier, *2001*, Analyses of the stress field in Southeastern France from earthquake focal mechanisms, Geophys. J. Int., 145, 336-348.

[8] Barruol G., Deschamps A., and O. Coutant, *2004*, Mapping upper mantle anisotropy beneath SE France by SKS splitting indicates Neogene asthenospheric flow induced by Apenninic slab roll-back and deflected by the deep Alpine roots. Tectonophysics, 394, 125-138, doi:10.1016/j.tecto.2004.08.002.

[9] Ben Ismail W., and D. Mainprice, *1998*, An olivine fabric database: an overview of upper mantle fabrics and seismic anisotropy, Tectonophysics, 296, 145-158.

[10] Buttles J., and P. Olson, *1998*, A laboratory model of subduction zone anisotropy, Earth Planet. Sci. Lett., 164, 245-262.

[11] Carmignani L., Decandia F. A., Fantozzi P. L., Lazzarotto A., Liotta D., and M. Meccheri, *1994*, Tertiary extensional tectonics in Tuscany (Northern Apennines, Italy), Tectonophysics, 238, 1-4, 295-315.

[12] Carmignani L. and R. Kligfield, *1990*, Crustal extension in the Northern Apennines, the transition from compression to extension in the Alpi Apuane core complex, Tectonics, 9, 29, 1275-1303.

[13] Chiarabba C., Jovane L. and R. Di Stefano, *2005*, A new view of Italian seismicity using 20 years of instrumental recordings, Tectonophysics, 395, 251-268.

[14] Cucci L., Pondrelli S., Frepoli A., Mariucci M.T., and M. Moro, *2004*, Local pattern of stress field and seismogenic sources in the Pergola-Melandro basin and the Agri valley (Southern Italy), Geophys. J. Int., 156 (3), 575-583, doi:10.1111/j.1365246X.2004.02161.x.

[15] Delacou B., Sue C., Champagnac J. D., and M. Burkhard, *2004*, Present day geodynamics in the bend of the western and central Alps as constrained by earthquake analysis, Geophys. J. Int., 158, 753-774.

[16] Dewey J. F., Helman M. L., Turco E., Hutton D. H.W., and S. D. Knott, *1989*, Kinematics of Western Mediterranean, *in* Coward M. P., Dietrich D., Park R. G. (Eds), Alpine Tectonics, Vol. 45., Geological Society of London, Spec. Publ., 265-283.

[17] Dewey J. F., *1980*, Episodicity, sequence, and style at convergent plate boundaries, *in* The continental crust and its mineral deposits, edited by Strangway, D. W., Geological Association of Canada Special Paper 20, 553-573.

[18] Doglioni C., *1991*, A proposal for the kinematic modeling of W-dipping subductions-possible applications to the Tyrrhenian-Apennines system, Terra Nova, 3, 423-434.

[19] Dziewonski A.M., Chou T.-A., and J. H. Woodhouse, *1981*, Determination of earthquake source parameters from waveform data for studies of global and regional seismicity, J. Geophys. Res., 86, B4, 2825-2852.

[20] Earle P. S., and P. M. Shearer, *1994*, Characterization of global seismograms using an automatic-picking algorithm, Bull. Seismol. Soc. Am., 84, 366-376.

[21] Ekström G., and P. England, *1989*, Seismic strain rates in regions of distributed continental deformation, J. Geophys. Res., 94, 10231-10257.

[22] Ekström G., Dziewonski A.M., Maternovskaya N.N., and M. Nettles, *2005*, Global seismicity of 2003: centroid-moment tensor solutions for 1087 earthquakes, Phys. Earth Planet. Int., 148, 327-351.

[23] Eva E., and S. Pastore, *1993*, Revisione dei meccanismi focali dell'appennino settentrionale, Atti GNGTS, 12°Conv., Roma, pp. 147-159.

[24] Eva E., and S. Solarino, *1992*, Alcune considerazioni sulla sismotettonica dell'appennino nord-occidentale ricavate dall'analisi dei meccanismi focali, Studi Geol. Camerti, vol. Spec. 2, Append. Crop 1-1a, pp. 75-83.

[25] Eva E., and S. Solarino, *1998*,Variations of stress directions in the Western Alpine, Arc. Geophys., J. Int., 135, 438-448.

[26] Eva E., Solarino, S., Eva C., and C. Neri, *1997*, Stress tensor orientation derived from fault plane solutions in the Southwestern Alps, J. Geophys. Res., 102, 8171-8185.

[27] Faccenna C., Piromallo C., Crespo-Blanc A., Jolivet L., and F. Rossetti, *2004*, Lateral slab deformation and the origin of the western Mediterranean arcs, Tectonics, 23, TC1012, doi:10.1029/2002TC001488.

[28] Faenza L., Marzocchi W., and E. Boschi, *2003*, A nonparametric hazard model to characterize the spatio-temporal occurrence of large earthquakes; an application to the Italian catalogue, Geophys. J. Int. 155, 521-531.

[29] Frepoli A., and A. Amato, *1997*, Contemporaneous extension and compression in the Northern Apennines from earthquake fault-plane solutions, Geophys. J. Int., 129, 368-388.

[30] Frepoli A., and A. Amato, *2000*, Fault plane solutions of crustal earthquakes in Southern Italy (1988-1995): seismotectonic implications, Ann. Geofis., 43 (3), 437-467.

[31] Frohlich C., *1992*, Triangle diagrams: ternary graphs to display similarity and diversity of earthquake focal mechanisms, Phys. Earth Planet. Inter., 75, 193-198.

[32] Frohlich C., *2001*, Display and quantitative assessment of distributions of earthquake focal mechanisms, Geophys. J. Int., 144, 300-308.

[33] Gasparini C., Iannaccone, G., and R. Scarpa, *1985*, Fault-plane solutions and seismicity of the Italian Peninsula, Tectonophysics 117, 59-78.

[34] Gilbert F., and A. M. Dziewonski, *1975*, An application of normal mode theory to the retrieval of structural parameters and source mechanisms from seismic spectra, Philos. Trans. R. Soc. London, Ser.A, 278, 187-269.

[35] Hartog R., and S. Y. Schwartz, *2000*, Subduction-induced strain in the upper mantle east of the Mendocino triple junction, California, J. Geophys. Res., 105, 7909.

[36] Herak M., Herak, D., and S. Markusic, *1995*, Fault-plane solutions for earthquake (1956-1995) in Croatia and neighboring regions, Geofizika 12, 43-56.

[37] Hill K. and A. Hayward, *1988*, Structural constraints on the Tertiary plate tectonic evolution of Italy, Marine and Petroleum Geology, 5, 2-16.

[38] Jackson J., and D. P. McKenzie, *1988*, The relationship between plate motions and seismic moment tensors, and the rates of active deformation in the Mediterranean and Middle East, Geophys. J. Int., 93, 45-73.

[39] Jolivet L., Goffé B., Monié P., Truffert-Luxey C., Patriat M., and M. Bonneau, *1996*, Miocene detachment in Crete and exhumation P-T-t paths of high-pressure metamorphic rocks, Tectonics, 15, 1129-1153.

[40] Jolivet L., Faccenna C., Goffe B., Mattei M., Rossetti F., Brunet C., Storti F., Funiciello R., Cadet J., D'Agostino N., and T. Parra, *1998*, Midcrustal shear zones in postorogenic extension; example from the northern Tyrrhenian Sea, J. Geophys. Res., 103, B6, 12,123-12,160.

[41] Yu Y., and J. Park, *1993*, Upper mantle anisotropy and coupled-mode long-period surface waves, Geophys. J. Int., 114, 473-489.

[42] Kagan Y. Y., *1991*, 3-D rotation of double-couple earthquake sources, Geophys. J. Int., 106, 709-716.

[43] Karato S., *1987*, Seismic anisotropy due to lattice preferred orientation of minerals: Kinematic or dynamic?, *in* High-Pressure Research in Mineral Physics, Geophys. Monogr. Ser., vol. 39, edited by M. H. Manghnani and S. Syono, pp. 455-471, AGU, Washington, D. C.

[44] Karato S., and P. Wu, *1993*, Rheology of the upper mantle:A synthesis, Science, 260, 771-778.

[45] Kostrov V. V., *1974*, Seismic moment and energy of earthquakes, and seismic flow of rocks, Izv. Acad. Sci. USSR Phys. Solid Earth, 1, 23-44.

[46] Levin V., Menke W., and J. Park, *1999*, Shear wave splitting in the Appalachians and Urals: a case of multilayered anisotropy, J. Geophys. Res., 104, D8, 17,975-17,993.

[47] Levin V., Margheriti L., Park J., and A. Amato, *2002*, Anisotropic seismic structure of the lithosphere beneath the adriatic coast of italy constrained with mode-converted body waves, Geophys. Res. Lett., doi:10.1029/2002GL015438.

[48] Lister G.S., Banga G. and A. Feenstra, *1984*, Metamorphic core complexes of the Cordilleran type in the Cyclades, Aegean Sea, Geology, 12, 221-225.

[49] Lucente F. P., Chiarabba C., Cimini G., Giardini D., *1999*, Tomographic constraints on the geodynamic evolution of the Italian region, J. Geophys. Res., 104, 20307-20327.

[50] Lucente F. P., Margheriti L., Piromallo C., Barruol G., *2006*, Seismic anisotropy reveals the long route of the slab through the western-central Mediterranean mantle, Earth Planet. Sci. Lett., 241, 517-529.

[51] Mainprice D., and P. G. Silver, *1993*, Interpretation of SKS-waves using samples from the subcontinental lithosphere, Phys. Earth Planet. Inter., 78, 257-280.

[52] Makris J., Egloff F., Nicolich R., and R. Rihm, *1999*, Crustal structure from the Ligurian Sea to the Northern Apennines-a wide angle seismic transect, Tectonophysics, 301, 305-319.

[53] Malinverno A., and W. Ryan, *1986*, Extension in the Tyrrhenian Sea and shortening in the Apennines as result of arc migration driven by sinking of the lithosphere, Tectonics, 3, 18, 227-245.

[54] Margheriti L., Nostro C., Cocco M., Amato A., *1996*, Seismic anisotropy beneath the Northern Apennines (Italy) and its tectonic implications, Geophys. Res. Lett., 23, 2721-2724.

[55] Margheriti L., Lucente F. P., and S. Pondrelli, *2003*, SKS splitting measurements in the Apenninic-Tyrrhenian domain (Italy) and their relation with lithospheric subduction and mantle convection, J. Geophys. Res., 108, B4, 2218, doi:10.1029/2002JB001793.

[56] Margheriti L., Pondrelli S., Piccinnini D., Piana Agostinetti N., Giovani L., Salimbeni S., Lucente F. P., Amato A., Baccheschi P., Park J., Brandon M., Levin V., Plomerová J., Jedlicka P., Vecsey L., Babuška V., Fiaschi A., Carpani B., and Ulbricht P., *2007*, The subduction structure of the Northern Apennines: results from RETREAT Seismic Deployment, Annals of. Geophysics, 49, 4/5, August/October.

[57] Mele G., and E. Sandvol, *2003*, Deep crustal roots beneath the northern Apennines inferred from teleseismic receiver functions, Earth Planet. Sci. Lett. 211, 69-78.

[58] Menke W., and V. Levin, *2003*, The cross-convolution method for interpreting SKS splitting observations, with application to one and two-layer anisotropic earth models, Geophys. J. Int., 154, 379-392.

[59] Molnar P., *1983*, Averange regional strain due to slip on numerous faults of different orientations, J. Geophys. Res., 88, 6430-6432.

[60] Molnar P., England P., and J. Martinod, *1993*, Mantle dynamics, the uplift of the Tibetan Plateau, and the Indian monsoon, Reviews of Geophysics, 31, 357-396.

[61] Montone P., Amato A., and S. Pondrelli, *1999*, Active stress map of Italy, J. Geophys. Res., 104, B11, 25,595-25,610.

[62] Montone P., Mariucci M.T., Pondrelli S., and A. Amato, *2004*, An improved stress map for Italy and surrounding regions (Central Mediterranean), J. Geophys. Res. 109, 10410, doi:10.1029/2003JB002703.

[63] Morgante A., M. R. Barchi, S. D'Offizi, G. Minelli, and G. Pialli, *1998*, The contribution of seismic modeling to the interpretation of the CROP 03 line, Results of the CROP03 deep seismic reflection profile, Memorie della Societa Geologica Italiana, 52, 441-455.

[64] Muço B., *1994*, Focal mechanism solutions for Albanian earthquakes for the years 1964-1988, Tectonophysics 231, 311-323.

[65] Nicolas M., Santoire J. P., and P. Y. Delpech, *1990*, Intraplate seismicity: new seismotectonic data in Western Europe, Tectonophysics, 179, 27-53.

[66] Ori G. G., and P. F. Friend, *1984*, Sedimentary basins formed and carried piggy-back on active thrust sheets, Geology, 12, 475-478.

[67] Özalaybey S., and M. K. Savage, *1994*, Double-layer anisotropy resolved from S phases, Geophys. J. Int., 117, 653-664.

[68] Patacca E., R. Sartori, and P. Scandone, *1990*, Tyrrhenian Basin and Apenninic arcs; kinematic relations since late Tortonian times, Memorie della Societá Geologica Italiana, 45, 425-451.

[69] Pauselli C., M.-R. Barchi, C. Federico, M. B. Magnani, and G. Minelli, *2006* , The crustal structure of the northern Apennines (central Italy): an insight by the CROP03 seismic line, Am. J. Sci. 306, 428-450.

[70] Pearce J., and D. Mittleman, *2002*, Defining the Fresnel zone for broadband radiation, Phys. Rev., 66, 056602, doi:10.1103/PhysRevE.66.056602.

[71] Piana Agostinetti N., F. P. Lucente, G. Selvaggi, and M. Di Bona, *2002*, Crustal structure and Moho beneath the Northern Apennines (Italy), Geophys. Res. Lett. 29 (20), doi:10.1029/2002GL015109.

[72] Piccotti V., and F. J. Pazzaglia, *2008*, A new active tectonic model for the construction of the Northern Apennines mountain front near Bologna (Italy), submitted.

[73] Pini G. A., *1999*, Tectonosomes and olistostromes in the argille scagliose of the Northern Apennines, Italy, Geological Society of America Special Paper 335, 70 pp.

[74] Piromallo C., and A. Morelli, *2003*, P wave tomography of the mantle under the Alpine-Mediterranean area, J. Geophys. Res., 108 (B2), doi:10.1029/2002JB001757.

[75] Plomerová J., Babuška, V., Šilený J., and J. Horálek, *1998*, Seismic anisotropy and velocity variations in the mantle beneath the Saxothuringicum-Moldanubicum contact in central Europe, Pure appl. Geophys., 151, 365-394

[76] Plomerová J., Margheriti L., Park J., Babuška V., Pondrelli S., Vecsey L., Piccinini D., Levin V., Baccheschi P., and S. Salimbeni, *2006*, Seismic anisotropy beneath the Northern Apennines (Italy): Mantle flow or lithosphere fabric?, Earth Planet. Sci. Lett., 247, 157-170.

[77] Pondrelli S., Morelli A., Boschi E., *1995*, Seismic deformation in the Mediterranean area estimated by moment tensor summation, Geophys.J.Int., 122, 938-952.

[78] Pondrelli S., Ekström G., Morelli A., Primerano, S., *1999*, Study of source geometry for tsunamigenic events of the Euro-Mediterranean area, International Conference on Tsunamis, UNESCO books, Paris, pp. 297-307.

[79] Pondrelli S., Ekström G., Morelli A., *2001*, Seismotectonic re-evaluation of the 1976 Friuli, Italy, seismic sequence, J. Seismol., 5, 73-83.

[80] Pondrelli S., Morelli A., Ekstrom G., Mazza S., Boschi E., Dziewonski A. M., *2002*, European-Mediterranean regional centroid-moment tensors: 1997-2000, Phys.Earth Planet.Inter., 130, 71-101.

[81] Pondrelli S., Morelli A., and Ekström G., *2004a*, European-Mediterranean regional centroid-moment tensor catalog: solutions for years 2001 and 2002, Phys. Earth Planet. Int., 145 (1-4), 127-147.

[82] Pondrelli S., Piromallo C., and E. Serpelloni, *2004b*, Convergence vs. retreat in Southern Tyrrhenian Sea: insights from kinematics, Geophys. Res. Lett., 31, 6, doi:10.1029/2003GL019223.

[83] Pondrelli S., Salimbeni S., Ekström G., Morelli A., Gasperini P., and G. Vannucci, *2006*, The Italian CMT dataset from 1977 to the present, Phys. Earth Planet. Int., 159, 286-303.

[84] Pondrelli S., Salimbeni S., Morelli, A., Ekström, G., and E. Boschi, *2007*, European-Mediterranean regional centroid-moment tensor catalog: solutions for years 2003 and 2004, Phys. Earth Planet. Int., 164, 90-120.

[85] Ponziani F., R. de Franco, G. Minelli, G. Biella, C. Federico, and G. Pialli, *1995*, Crustal shortening and duplication of the Moho in the Northern Apennines; a view from seismic refraction data, *in* Interplay of extension and compression in basin formation, edited by Cloetingh, S., B. D'Argenio, R. Catalano, F. Horvath, W. Sassi, Tectonophysics, 252, 391-418.

[86] Rümpker G., and P.G. Silver, *1988*, Apparent shear-waves splitting parameters in the presence of vertically varying anisotropy, Geophys. J. Int., 149, 313-327.

[87] Reddy S. M., Wheeler J. and R. A. Cliff, *1999*, The geometry and timing of orogenic extension; an example from the Western Italian Alps, J. Metamorphic Geol., 17, 5, 573-589.

[88] Renner G., and D. Slejko, *1986*, Studio di alcuni recenti terremoti dell'Italia nord orientale in un contesto sismotettonico regionale, Atti GNGTS, 5°Conv., Roma, 577-589.

[89] Renner G., and D. Slejko, *1994*, Some comments on the seismicity of the Adriatic Region, Boll. Geof. Teor. Appl., XXXVI, 141-144.

[90] Ribe N. M., *1989*, Seismic anisotropy and mantle flow, J. Geophys. Res., 94, 4213-4223.

[91] Ricci Lucchi F., *1986*, The foreland basin system of the Northern Apennines and related clastic wedges; a preliminary outline, *in* Paleogeography and geodynamics of the peri-Tyrrhenian area; proceedings, edited by Boccaletti, M., R. Gelati, F. Ricci Lucchi, Giornale di Geologia 48, 165-185.

[92] Royden L. H., *1993*, Evolution of retreating subduction boundaries formed during continental collision, Tectonics, 12, 3, 629-638.

[93] Russo R. M., and P. G. Silver, *1994*, Trench-parallel flow beneath the Nazca plate from seismic anisotropy, Science, 263, 1105-1111.

[94] Salimbeni S., Pondrelli S., Margheriti L., Levin V., Park J., Plomerová J., and Babuška V., *2007*, Abrupt change in mantle fabric across northern Apennines detected using seismic anisotropy, Geoph. Res. Lett., 34, L07308, doi:10.1029/2007GL029302.

[95] Salimbeni S., Pondrelli S., Margheriti L., Park J., and V. Levin, *(*2008), SKS splitting measurements beneath Northern Apennines region: a case of oblique trench retreat, submitted.

[96] Saltzer R. L., Gaherty J. B., and T. H. Jordan, *2000*, How are shear-wave splitting measurements affected by variations in the anisotropy with depth?, Geophys. J. Int., 141, 374.

[97] Sandvol E., and T. Hearn, *1994*, Bootstrapping shear-wave splitting errors, Bull. Seismol. Soc. Am., 84, 1971-1977.

[98] Savage M. K., *1999*, Seismic anisotropy and mantle deformation: what have we learned from shear wave splitting?, Rev. of Geophys., 37, 65-106.

[99] Scrocca D., E. Carminati, C. Doglioni, and D. Marcantoni, *2007*, Slab retreat and active shortening along the Central-Northern Apennines, *in* Lacombe, O., Roure, F. (eds), Thrust belts and foreland basins, from fold kinematics to hydrocarbon system, Springer Verlag, chapt. 25, 18 pp.

[100] Selvaggi G., and A. Amato, *1992*, Subcrustal earthquakes in the northern Apennines (Italy): evidence for a still active subduction?, Geophys. Res. Lett., 19(21), 2127-2130.

[101] Selvaggi G., *2001*, Strain pattern of the Southern Tyrrhenian Slab from moment tensors of deep earthquakes: implications on the down-dip velocity, Ann. Geofis. 44 (1), 155-165.

[102] Serpelloni E., Anzidei M., Baldi P., Casula G., and A. Galvani, *2005*, Crustal velocity and strain-rate fields in Italy and surrounding regions: new results from the analysis of permanent and nonpermanent GPS networks, Geophys. J. Int. 161, 861-880.

[103] Shearer P., *1991*, Imaging global body wave phases by stacking long-period seismograms, J. Geophys. Res., 96, 20,353-20,364.

[104] Šilený J., and J. Plomerová, *1996*, Inversion of shear-wave splitting parameters to retrieve three-dimensional orientation of anisotropy in continental lithosphere, Phys. Earth Planet. Inter., 95, 277-292.

[105] Silver P. G., *1996*, Seismic anisotropy beneath the continents: Probing the depth of geology. Annu. Rev. Earth Planet. Sci., 24, 385-432.

[106] Silver P. G., and M. K. Savage, *1994*, The interpretation of shear wave splitting parameters in presence of two anisotropic layers, Geophys. J. Int., 119, 949-963.

[107] Silver, P. G., and W. W. Chan, *1988*, Implications for continental structure and evolution from seismic anisotropy, Nature, 335, 34-39.

[108] Silver P. G., and W. W. Chan, *1991*, Shear-wave splitting and subcontinental mantle deformation, J. Geophys. Res., 96(B16), 16429-16454.

[109] Spakman W., S. van der Lee, and R. van der Hilst, *1993*, Travel-time tomography of the European-Mediterranean mantle down to 1400 km, Phys. Earth Planet. Inter., 79, 3-74.

[110] Stein S. and G. F. Sella, *2006*, Pleistocene change from convergence to extension in the Apennines as a consequence of Adria microplate motion, *in* The Adria Microplate: GPS Geodesy, Tectonics, and Hazards, edited by Pinter, N. and Grenerczy, G., NATO Science Series, 61, Springer Netherlands, 21-34.

[111] Sue C., Thouvenot F., Frechet J., and P. Tricart, *1999*, Widespread extension in the core of the Western Alps revealed by earthquake analysis, J. Geophys. Res., 104, 25611-25622.

[112] Vannucci G., and P. Gasperini, *2003*, A database of revised fault plane solutions for Italy and surrounding regions, Computers & Geosciences, 29, 903-909.

[113] Vannucci G., and P. Gasperini, *2004*, The new release of the database of Earthquake Mechanisms of the Mediterranean Area (EMMA Version 2), Ann. Geophys., 47 (Suppl. 1), 307-334.

[114] Vannucci G., Pondrelli S., Argnani A., Morelli A., Gasperini P., and E. Boschi, *2004*, An atlas of Mediterranean seismicity, Ann. Geophys. 47, 247-306.

[115] Vinnik L. P., Kosarev G. L., and L. I. Makeyeva, *1984*, Anisotrope in the lithosphere from the observations of SKS aizd SKKS, Dokl. Akad. Nauk USSR, 278, 1335-1339 (in Russian).

[116] Wenk H.-R., G. Canova, A. Molinari, and U. F. Kocks, *1989*, Viscoplastic modeling of texture development in quartzite, J. Geophys. Res., 94, 17,895-17,906.

[117] Wessel P., and W. H. F. Smith, *1998*, New, improved version of Generic Mapping Tools released (version 3.1), EOS Trans. AGU, 79. 687

[118] Westaway R., *1992*, Seismic moment summation for historical earthquakes in Italy: tectonic implications, J. Geophys. Res., 97,15437-15464.

[119] Wortel M. J. R., and Spakman W., *1992*, Structure and dynamics of subducted lithosphere in the Mediterranean region, Proc. K. Ned. Akad. Wet., 95(3), 325-347.

[120] Zattin M., V. Picotti, and GG. Zuffa, *2002*, Fission-track reconstruction of the front of the Northern Apennine thrust wedge and overlying Ligurian unit, Am. Journ. Sci., 302, 346-379.

[121] Zhang S., and S.-I. Karato, *1995*, Lattice preferred orientation of olivine aggregates deformed in simple shear, Nature, 375, 774-777.

[122] Zoback M. L., *1992*, First-and second-order patterns of stress in the lithosphere: the world stress map project, J. Geophys. Res., 97, 11703-11728.

ACKNOWLEDGMENTS

I am grateful to Lucia Margheriti, Vadim Levin, Jeffrey Park and Gianfranco Vannucci for your useful revisions and for they helpful suggestion. A special thank is for Silvia Pondrelli for her patience. We use GMT software (WESSEL AND SMITH, 1998) to prepare the maps.